Summer 2021

Dissolved Nitrogen Cycling in the Eastern Canadian Arctic Archipelago From Stable Isotopic Data

Holly Westbrook

DISSOLVED NITROGEN CYCLING IN THE EASTERN CANADIAN ARCTIC ARCHIPELAGO FROM STABLE ISOTOPIC DATA

by

Holly Westbrook

Bachelor of Science
University of Connecticut, 2017

Submitted in Partial Fulfillment of the Requirements

For the Degree of Master of Science in

Marine Science

College of Arts and Sciences

University of South Carolina

2021

Accepted by:

Annie Bourbonnais, Major Professor

Susan Lang, Committee Member

Erik Smith, Committee Member

Julie Granger, Committee Member

Tracey L. Wedon, Interim Vice Provost and Dean of the Graduate School

DEDICATION

Dedicated to my nephews, Thomas and Diego León, to my dog, Jack, and to Prima.

ACKNOWLEDGEMENTS

I'd like to first acknowledge my funding from the National Science Foundation (NSF) (award #1927755 to Bourbonnais). I'd also like to give a huge thank you to my advisor, Dr. Annie Bourbonnais, for all her support and help through the many twists and turns in this project. I'm grateful to Dr. Cara Manning, Dr. Mohamed Ahmed, Dr. Brent Else, Dr. Phillipe Tortell, and Robert Izett for their assistant in sample collection and analysis, as well as Dr. Nadine Lehmann for providing the code used for station maps in this document. Additionally, I'd like to thank my committee for their input and advice. I would like to acknowledge that sample collection took place off the shores and within the rivers of Inuit, Inughuit Nunaat, and Kalaallit Nunaat land, and samples were analyzed on Congaree and Tsalaguwetiyi land. I thank the crew of the CCGS Amundsen and ArcticNet for making this research possible. I'm also very grateful to the small army of undergraduates who have helped me: Darcy Perin, Maggie Gaspar, Elise Lumsden, Adrianna Webb, Jaquan High, and Miles Hampton. To my isotope friends, Lindsey Potts and Peter Ruffino, thank you for always talking over ideas with me and letting me know whether or not I am crazy. To Lynn, thank you for always listening to and helping me with my coding problems. To my non-isotope friends, thank you for bearing with me the past two years. To my cohort, it's been a pleasure, I wish we could have hung out more but that's just life in a pandemic. And finally, to my parents and sisters, thank you for supporting me emotionally, and for sending me wine money in my many times of need.

ABSTRACT

Climate change is expected to drastically alter the input of inorganic nitrogen (N) sources in the Eastern Canadian Arctic Archipelago (ECAA) with increasing discharge from glacial meltwater and permafrost thawing. Since dissolved inorganic N is generally depleted in surface waters, dissolved organic N (DON) could represent a significant source of nutrients limiting primary production in Arctic ecosystems. Yet, few DON data for this region exist. We analyzed stable isotopes ($\delta^{15}N$ and $\delta^{18}O$ of DON and NO_3^-) to investigate dissolved nitrogen cycling in glacial rivers and marine surface samples collected in the ECAA during summer 2019. We used isotopic data to determine dissolved N sources as well as production and consumption processes. DON concentrations (0.54-11.61 μmol L^{-1}) and $\delta^{15}N$ of DON (-0.71-9.61 ‰) in the ECAA were variable between different locations, suggesting the occurrence of different processes. DON concentrations were low in most rivers (up to 4.89 μmol L^{-1}). DON concentrations versus salinity fell along a mixing line between low DON riverine and higher DON marine end members. Thus, increased input from glacial meltwater in the ECAA could act to increase stratification and dilute the marine DON pool, ultimately affecting primary productivity. In regions of highest primary productivity, DON concentrations were inversely correlated with chlorophyll-a and the $\delta^{15}N$ of DON, suggesting net DON consumption during these localized phytoplankton blooms. We derived an isotope effect of -6.9‰ during DON consumption. Our data helps establish a baseline to assess future change in nutrient regime for this climate sensitive region.

TABLE OF CONTENTS

LIST OF TABLES

LIST OF FIGURES

LIST OF SYMBOLS

δ Delta notation in units of per mille (‰): $\delta^{15}N$ or $\delta\,^{18}O = [(R_{sample}/R_{standard}) -1] \times 1000$.

k Equilibrium constant for reactions involving the exchange of isotopes.

ε Kinetic isotope effect for non-equilibrium reactions:
$\varepsilon = [(^{light}k/^{heavy}k)-1] \times 1000)$

$\Delta(15,18)$ N-to-O isotope anomaly quantified as the deviation relative to a 1:1 fractionation relationship with a slope ($^{18}e/^{15}e$) of 1 during pure assimilatory and dissimilatory nitrate reduction

LIST OF ABBREVIATIONS

DIN ..... Dissolved Inorganic Nitrogen

DO ..... Dissolved Oxygen

DON ..... Dissolved Organic Nitrogen

ECAA ..... Eastern Canadian Arctic Archipelago

HDPE ..... High-density Polyethylene

HPLC ..... High Performance Liquid Chromatography

POR ..... Persulfate Oxidizing Reagent

TDN ..... Total Dissolved Nitrogen

VSMOW ..... Vienna Standard Mean Ocean Water

CHAPTER 1

INTRODUCTION

Climate change is rapidly altering Arctic ecosystems; as air and seawater temperatures are rising, sea ice melting and river discharges are increasing (Bintanja & Selten, 2014; Wassmann et al., 2011; Wu et al., 2005). The critical roles played by the Arctic Ocean in controlling the thermohaline circulation and fisheries greatly stimulated scientific research in the region within the past few decades. While primary productivity is expected to increase in the Western Arctic, similar changes are not ubiquitous across the entire Arctic. For example, decreased nutrient delivery through physical circulation as well as increased stratification due to higher freshwater input may overall decrease primary productivity in the Eastern Canadian Arctic Ocean (Granger et al., 2018; Lehmann et al., 2019). Nutrients in the surface waters of this region are typically low unless there is a localized nutrient source, such as buoyancy-driven upwellings in proximity to Greenland Ice Sheet (Cape et al., 2019). The availability of nutrients, as well as access to sunlight, are the key factors controlling Arctic primary productivity (Tremblay et al., 2015). Nitrogen is often limiting in the Arctic (Tremblay et al., 2006; Yamamoto-Kawai et al., 2006) and thus sources and sinks of nitrogen need to be constrained to better understand the current N budget as a baseline to assess future changes.

Dissolved organic nitrogen (DON) is the largest pool of fixed nitrogen in aquatic systems. The rate at which DON is utilized depends on the lability of the DON pool and the type of microorganisms present, as not every microorganism has the proper enzymes or mechanisms to take up DON (Sipler & Bronk, 2014). DON has been overlooked in the past as it was assumed to be too refractory and only utilized by bacteria (Berman & Bronk, 2003). However, labile DON was shown to be an essential source of N to primary producers, especially in N limited regions (Bronk et al., 2007; Knapp et al., 2018; Moschonas et al., 2017; Thibodeau et al., 2017). DON is composed of a highly refractory pool, and a smaller labile pool, such as amino acids or DNA, which can be utilized on time scales ranging from hours to years. DON can be produced *in situ* in the oceans through mechanisms such as the viral lysing of bacteria or the loss of prey biomass during feeding by microzooplankton (Sipler & Bronk, 2014). However, rivers are one of the major sources due to the presence of terrestrial organic matter. As a result, DON tends to be higher in coastal areas than in the open ocean, although the utilization of DON is not limited to coastal regions (Knapp et al., 2018; Letscher et al., 2013). DON can be produced in productive areas and then transported out into N limited regions; this process can fuel primary production when the more bioavailable inorganic forms of nitrogen are absent (Knapp et al., 2018; Letscher et al., 2013).

Despite its potential importance in N limited regions such as the Arctic, DON in the Eastern Canadian Arctic Archipelago (ECAA) is largely understudied with regards to sources and sinks. The surface Arctic Ocean has an average DON concentration of 4.7 μmol N L^{-1}, which is considerably less than the concentration in major Arctic rivers, which ranges from 7.4-18.4 μmol N L^{-1} (Sipler & Bronk, 2014). The Arctic region is

heavily impacted by rivers, as it receives 10% of global river discharge (Holmes et al., 2012). The fate of this riverine DON in coastal marine waters is still unclear, whether it is being utilized, or simply diluted through mixing with DON deplete waters. Tank et al. (2012) found that overall riverine DON in the Arctic is slowly remineralized, representing a significant source of bioavailable N to the open ocean. They also suggest that riverine DON can support localized coastal primary production. Thibodeau et al. (2017) also found that DON discharged of the Lena River in the Eurasian Arctic was rapidly consumed, with over 50% of it disappearing before reaching the shelf. Further confounding our understanding of DON cycling in the Arctic, Dittmar et al. (2001) found that DON input from Siberian rivers did not substantially support primary productivity, as it was largely recalcitrant. With riverine discharge increasing since around the 1960s (Peterson et al., 2002; Wu et al., 2005), these previous studies highlight the need to further understand the extent to which rivers influence the delivery of bioavailable DON in Arctic coastal waters.

There are other potential sources of Arctic nutrients in addition to rivers such as glacially-driven upwelling and glacial melt. Glacial upwelling supplies nutrients to the Arctic surface waters, as seen with the Greenland Ice Sheet (Cape et al., 2019). While the supply of inorganic nutrients such as nitrate, silicate, and phosphate, has been identified through this process, DON was not investigated. However, upwelling regions generally see elevated DON concentrations following the increase in biological activity due to NO_3^- input from below (Sipler & Bronk, 2014). Since most rivers are of glacial origin in the ECAA, both glacial versus terrestrial riverine end members must be constrained in order to identify the sources and fate of DON in this rapidly changing region.

Stable isotopes of N and O in N species are used to disentangle N transformations as organisms preferentially assimilate lighter isotopes. The nitrogen $^{15}N/^{14}N$ isotope ratios are reported in delta notation (δ) and units of per mille (‰), where the $^{15}N/^{14}N$ and $^{18}O/^{16}O$ references are air for is N_2 and Vienna Standard Mean Ocean Water (VSMOW) for O.

$$\delta^{15}N = [(^{15}N/^{14}N_{sample}/ {}^{15}N/^{14}N_{air}) - 1] \times 1000$$

$$\delta^{18}O = [(^{18}O/^{16}O_{sample}/ {}^{18}O/^{16}O_{VSMOW}) - 1] \times 1000$$

The $\delta^{15}N$ of DON is influenced by the $\delta^{15}N$ of its source. Therefore, $\delta^{15}N$ DON can be a strong indicator of the dominant source of new N in a system, such as the input of low ^{15}N- ammonium (NH_4^+; -2 to 0‰) from N_2 fixation (Carpenter et al., 1997; Minagawa & Wada, 1986 as in Knapp et al., 2018). Conversely, the $\delta^{15}N$ DON released by phytoplankton could also be elevated if the assimilated substrate (NO_3^- and NO_2^-) was partially denitrified, due to kinetic isotopic fractionation that leaves the residual substrate with a relatively high $\delta^{15}N$ (Knapp et al., 2018; Knapp et al., 2005). Alternatively, DON produced through newly regenerated N, typically NH_4^+, will often have a lower $\delta^{15}N$ as lighter isotopes are preferentially excreted (Fawcett et al., 2011).

Additionally, the $\delta^{18}O$ of NO_3^- can be used to disentangle NO_3^- production, consumption, and input. During nitrification, at least 2/3 of O atoms in NO_3^- come from water, with oxygen isotopic fractionation and exchange with water during bacterial ammonia and nitrite oxidation (Buchwald et al., 2012; Casciotti et al. 2010). We can thus estimate the end member for newly nitrified NO_3^- based on the $\delta^{18}O$ of water and DO as well as the isotope effects and exchange with water during ammonium and nitrite

oxidation. On the other hand, NO_3^- assimilation, introduces an isotope effect on both $\delta^{18}O$ and $\delta^{15}N$ in a 1:1 ratio (Granger et al., 2004). This relationship can be used to determine the influence of processes other than pure assimilation on the NO_3^- pool.

The $\delta^{18}O$ of water and salinity can be used to differentiate DON supplied from freshwater sources from marine sources, as freshwater, marine water, and sea ice melt all have unique salinities and $\delta^{18}O$ of water. The freshwater end member includes both glacial and terrestrial riverine water, as they have very similar values. These parameters can be applied to a mixing model to constrain the relative contribution from marine, riverine, glacial, and sea ice melt end members.

The goals of this study are to determine, using an isotopic approach, 1) the sources of DON and 2) how DON from glaciers or rivers is consumed as it is transported offshore. This study focuses on the Nares Strait, Jones Sound, Lancaster Sound, and Baffin Bay, whose coastal regions are more extensively covered by glaciers compared to other Arctic regions. This region of the Arctic also experiences high permafrost coverage. Nutrient input from other sources, such as terrestrial rivers, are more significant in other Arctic regions such as the Laptev Sea and the western Arctic. The Eastern Baffin Bay is a highly productive area important for fisheries in Greenland. Determining the sources of DON input to coastal waters is essential to predict the effect of climate change on primary productivity in these economically important regions.

CHAPTER 2

METHODS

2.1 SAMPLE LOCATION AND COLLECTION

Samples were collected during Leg 2a and 2b of the ArcticNet expedition aboard the CCGS *Amundsen* from July 5th to August 15th of 2019. The expedition took place in the ECAA in Baffin Bay, the Nares Strait, Lancaster Sound, and Jones Sound. Sampling locations are presented in Figure 2.1. The prevailing currents of this region come from the north, through the Nares Strait, into the Kane Basin, Smith Sound, and finally into Baffin Bay. Additionally, currents flow from Lancaster Sound into Baffin Bay from the west. In the surface, these water masses are Pacific generated and circulate in the Canadian and Makarov Basins before entering the ECAA. In Baffin Bay, Atlantic water enters from the southwestern coast of Greenland and travels north until it converges with water flowing south from the Smith Sound and circulates southwards on the eastern side of Baffin Island (Granger et al., 2018; Tang et al., 2004). Atlantic water can be found at depth in Baffin Bay (Alkire et al., 2010). Circulation in the study area is depicted in Figure 2.1. Ice cover in this region varies by season, with the lowest coverage in the summer (Tang et al., 2004). Ice in Baffin Bay is mostly formed in the Nares Strait and transported south. Ice formed in other channels is typically blocked by landfast ice and does not enter Baffin Bay (Tang et al., 2004).

Samples for DON analysis were collected using 12L Niskin bottles at depths of 100 m and 80 m, and then upwards to the surface in 10 m intervals. Samples at 100 and 80 m were collected in 15 mL centrifuge tubes, and samples taken above 80 m were collected in 60 mL HDPE plastic bottles. All bottles were rinsed three times with sample water prior to collection. All samples were frozen with a headspace to allow for water expansion upon freezing, until analysis. Samples taken during Leg 2b were also filtered with GF/F filters before freezing. Leg 2a samples were filtered prior to analysis with Supor^{TM} 0.45 micron polyethersulfone filters. A comparison was performed on the effect of the different filters on [DON] and $\delta^{15}N$ DON—no significant difference was observed. Riverine samples were collected from the surface waters of 11 rivers, filtered with GF/F filters, and frozen. Water samples were also collected for $\delta^{18}O$ of H_2O analysis; samples were collected without bubbles in small glass vials and stored at room temperature.

2.2 CONCENTRATION AND ISOTOPIC ANALYSIS OF DON, NO_3^-, AND $\delta^{18}O$ OF H_2O

The [DON] and $\delta^{15}N$ of DON were measured as in Knapp et al. (2005). Briefly, TDN was oxidized to NO_3^- using recrystallized persulfate followed by measurement on a NO_x analyzer by chemiluminescent detection (Braman & Hendrix, 1989). [DON] was then estimated as the difference between TDN and DIN. The $\delta^{15}N$ of NO_3^- was then analyzed using the denitrifier method (Sigman & Casciotti, 2001).

As there is no mean to remove dissolved inorganic nitrogen, the combined concentration and isotopic composition of NO_3^- and NO_2^- (and NH_4^+ if present) must be analyzed to calculate the $\delta^{15}N$ of DON by isotopic mass balance. [NO_3^- + NO_2^-] was thus

also measured by chemiluminescence prior to persulfate oxidation and the $\delta^{15}N$ of NO_3^- only was determined using the denitrifier method (Casciotti et al., 2002; Sigman & Casciotti, 2001). [NO_3^-] and [NO_2^-] were also provided by Jean-Éric Tremblay lab group at Université Laval. Nitrite concentrations were generally below detection limit in our samples (less than 0.22 μM in marine samples and less than 1.36 μM in riverine samples). Only samples in which DON comprises over 50% of TDN were considered.

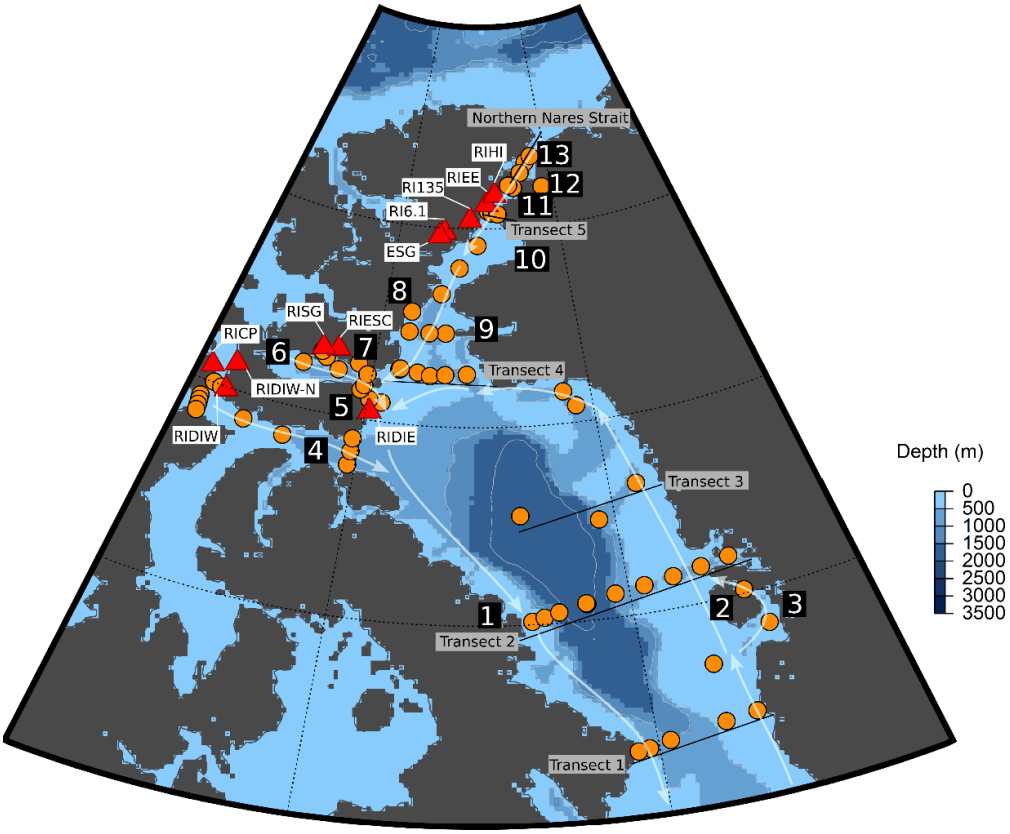

Figure 2.1: Map of the sampling locations. CTD casts are marked with orange circles. Red triangles represent river locations, which are also labeled by name. Transects 1, 2, 3, 4, 5, and the Northern Nares Strait are also labeled with solid black lines. The directions of surface currents are shown by the white arrows. Important regions and features numbered as follows: 1- Clyde River, 2- Disko Island, 3 – Jakobshavn Glacier, 4 – Lancaster Sound, 5 – Devon Island, 6 – Jones Sound, 7 – Manson Icefield, 8 – Talbot Inlet, 9 – Smith Sound, 10 – Kane Basin, 11 – Kennedy Channel, 12 – Petermann Glacier, 13 – Hall Basin. 8-13 are all considered part of Nares Strait.

Briefly, 1 mL of freshly prepared persulfate oxidizing reagent (POR) was added to 6 mL of sample in 12 mL threaded test tubes with Teflon-lined phenolic screw caps (Corning 99447-161). These samples were then autoclaved for one hour. POR blank was typically <0.4 μmol N L^{-1} and [TDN] was corrected for blank contribution. Additionally, 5 μmol N L^{-1} of the international standards USGS-40, USGS-64, and USGS-65 and an internal standard of 6-aminocarproic acid were analyzed with each run to verify oxidation efficiency and that no fractionation occurred during the persulfate oxidation step.

Prior to isotopic analysis, the pH of autoclaved samples, standards, and blanks were adjusted to 3-4 with 6N HCl. Neutralized samples were injected into 2 mL of *Pseudomonas chlororaphis* suspended in media. When analyzing NO_3^- alone, *Pseudomonas aureofaciens* was instead used in order to determine $\delta^{18}O$ of NO_3^-. In the few samples for which NO_2^- accumulated, NO_2^- was removed using sulfamic acid as in Granger & Sigman, (2009). The target sample size was 20 nmol. The product N_2O was purified and analyzed in continuous flow using an Elementar Americas PrecisION isotope ratio mass spectrometer equipped with a custom on-line gas extraction and purge-trap system and PAL autosampler. Samples were standardized using a two-point correction with the international standards IAEA N-3 ($\delta^{15}N$ = 4.7‰ vs air) and USGS-34 ($\delta^{15}N$ = -1.8‰ vs air). The $\delta^{15}N$ of DON was determined by isotopic mass balance taking into consideration the concentration and $\delta^{15}N$ of the POR blank as well as sample NO_3^- and TDN. The average standard deviation for duplicate $\delta^{15}N$-DON analysis was generally lower than ±0.5‰. Error propagation was determined using a Monte Carlo method as in Knapp et al. (2018).

The $\delta^{18}O$ of H_2O was measured using an integrated off-axis cavity absorption spectrometer (Los Gatos Research, LGR, Triple Liquid Water Isotope Analyzer, model 912-0032) at the University of Calgary as described in Ahmed et al. (2020).

Chlorophyll-a was also measured using High Performance Liquid Chromatography (HPLC) at the University of British Columbia as described in Burt et al. (2018). Surface stations and cross-sections were generated with the Ocean Data View software (Schlitzer, 2021).

2.3 MIXING MODEL

$\delta^{18}O$ of H_2O and salinity were used in the following simple mixing model in order to determine the relative contributions of marine water (*mar*), freshwater (*fw*), and sea ice melt (*sim*).

$$f_{mar} + f_{fw} + f_{sim} = 1$$

$$f_{mar} * S_{mar} + f_{fw} * S_{fw} + f_{sim} * S_{sim} = S_{measured}$$

$$f_{mar} * O_{mar} + f_{fw} * O_{fw} + f_{sim} * O_{sim} = O_{measured}$$

Wherein *f* is the fraction of each end member, *S* is salinity and *O* is $\delta^{18}O$ of H_2O. End member values used in the calculations are listed in Table 2.1. Note that because river and glacial end members have identical salinities and extremely similar $\delta^{18}O$ of H_2O values, -20 and -20.5-21.7‰ respectively (Bedard et al., 1981; Thibodeau et al., 2017), we cannot distinguish between these end members with this dataset. Therefore, we must look at the freshwater end member as a whole and use a value of -20 ‰ for our freshwater $\delta^{18}O$ end member. The contribution of sea ice melt can be considered in two

regards: as net sea ice melt or local sea ice melt. Net sea ice melt is integrated over time and reflects the difference between ice formation during the winter and ice melt during the spring and summer. Local sea ice melt is the instantaneous contribution of sea ice melt at the time of sampling. In both cases, a positive value indicates melting, and a negative value indicates formation. Because the melting and formation of sea ice are decoupled in time and space, the contribution of sea ice melt determined from the end members in Table 2.1 represents net sea ice melt rather than local sea ice melt. In order to determine local sea ice melt, we utilized a two-layer mixing model as in Alkire et al. (2010).

Table 2.1: End member values used in the mixing model.

End Member	**Salinity (PSU)**	**$\delta^{18}O$-H_2O (‰)**
Pacific Water	32.5	-0.8
Atlantic Water	34.87	0.24
Freshwater (Rivers & Glaciers)	0	-20
Sea Ice	4	0.05

Additionally, because this region has marine water originating from both the Pacific and Atlantic Oceans, we calculate our marine end members (S_{mar} and O_{mar}) based on the ratio of Pacific to Atlantic water. This ratio is calculated using the concentrations of NO_3^- and phosphate (Jones et al., 1998; Sherwood et al., 2021; Yamamoto-Kawai et al., 2008).

2.4 MODEL FOR RIVERINE NO_3^- CYCLING

We used a simple steady-state isotopic model to apportion the sources and sinks of NO_3^- in ECAA rivers. This model included two sources of NO_3^- supplied to glacial rivers NO_3^- from the nitrification of permafrost or atmospheric NH_4^+ (e.g., Alves et al., 2013; Fouché et al., 2020; Wagner et al., 2002) and 2) atmospheric deposition (e.g., Hastings et al., 2004). We assumed that nitrification of NH_4^+ adds NO_3^- with a $\delta^{15}N$ of ~1.22‰ (range: -6 and 10‰; (Ansari et al., 2013; Arendt et al., 2016; Heikoop et al., 2015; Louiseize et al., 2014; Wynn et al., 2007). The $\delta^{18}O$ produced during microbial oxidation of NH_4^+ was estimated to be ~-14.21‰, assuming that at least 2/3 of the O atoms are derived from water during nitrification (Casciotti et al., 2010; Heikoop et al., 2015). For this estimation, we assume the $\delta^{18}O$ of water ranges from -12‰ to -22 ‰ (Arendt et al., 2016; Wynn et al., 2007) and the $\delta^{18}O$ of dissolved oxygen could range from 23.7‰ to 24.2‰ based on the $\delta^{18}O$ of air (Kiddon et al., 1993; Wang & Veizer, 2000; Horibe et al., 1973 as in Wynn et al., 2007). Additionally, we assumed isotope effects on the $\delta^{18}O$ NO_3^- and exchange with H_2O during bacterial nitrification as in Buchwald et al. (2012) and Casciotti et al. (2010). We also assumed that any NH_4^+ was completely oxidized to NO_3^- in rivers, as NH_4^+ concentrations were below detection limit in our samples. We assumed that atmospheric deposition added NO_3^- with a $\delta^{15}N$ of -3.54‰ and a $\delta^{18}O$ of 72.07‰ (Ansari et al., 2013; Hastings et al., 2004; Heikoop et al., 2015; Louiseize et al., 2014). We assumed an N kinetic isotope effect (ε) of 5‰ (Altabet, 2001) and a $^{18}\varepsilon$:$^{15}\varepsilon$ of 1:1 during pure NO_3^- assimilation (Granger et al., 2004). The isotope effect is defined as $^{15}\varepsilon = (((^{14}k/^{15}k)-1) \times 1000)$, where ^{14}k and ^{15}k are the rate coefficients of the reactions for the light and heavy isotopes respectively. We excluded

denitrification, the canonical conversion of NO_3^- to the nitrogen gases N_2O and N_2 under anaerobic conditions, due to the high O_2 concentrations in the rivers (Dalsgaard et al., 2014).

We considered 2 main scenarios, the first with 45% recycled production, the second with 30% recycled production. More details can be found in Appendix A.

We used this model to reproduce the deviation from the $^{18}\varepsilon:^{15}\varepsilon$ ratio of ~1 observed for pure NO_3^- assimilation (Granger et al., 2004) of our riverine samples. We refer to this deviation as the $\Delta(15,18)$, which is the difference between NO_3^- $\delta^{15}N$ and $\delta^{18}O$ (Rafter et al., 2013).

2.5 ISOTOPE EFFECT OF DON CONSUMPTION

In areas where primary productivity was the highest and where net DON consumption was observed, we estimated the $^{15}\varepsilon$ of DON consumption using a closed system Rayleigh model ($\delta^{15}N$ of DON vs ln([DON])) as in Knapp et al. (2018). A low [DON] concomitant with elevated $\delta^{15}N$ indicates consumption, as kinetic isotope fractionation during consumption increases the $\delta^{15}N$ of the residual DON pool.

CHAPTER 3

RESULTS

3.1 PHYSICAL CHARACTERISTICS OF THE ECAA

Salinity and $\delta^{18}O$ of water were used to identify the physical characteristics of the study region. Upwelling was identified in the eastern part of Transect 1 and Transect 2 (Figure 3.1A & Figure 3.1B, respectively). Near shore waters were influenced by freshwater input from rivers and/or glacial meltwater. This is evident throughout the study region, with more distinct signals near Talbot Inlet, Petermann Glacier, Jakobshavn Glacier, within Lancaster sound, and near the riverine stations RISG and RIESC in Jones Sound. Figure 3.2A depicts the fraction of freshwater in surface waters of the study area. Stations closest to land have a higher fraction of freshwater, as expected. The low fraction of freshwater on the eastern coast of Transect 1 and 2 is attributed to upwelling as well as influence from the West Greenland Current, which is more saline than the Baffin Current (Alkire et al., 2010). Sea ice melt, shown in Figure 3.2B, was highest on the western side of Transect 2, which is close to the mouths of the Clyde river. Sea ice melt was also slightly higher in the Northern Nares Strait, Transect 1, as well as Lancaster and Jones Sounds. Sea ice formation was observed near the Jakobshavn Glacier, in Transect 3, and in Talbot Inlet; however, this could be due to uncertainties associated with the halocline end member $\delta^{18}O$ used to calculate the fraction of local sea ice melt. While the halocline end members for each individual station should ideally be

used in this calculation, we used the halocline end members for different regions provided in Alkire et al. (2010) due to limited spatial coverage for the $\delta^{18}O$ of H_2O measurements. This introduces some uncertainty in the sea ice melt contribution.

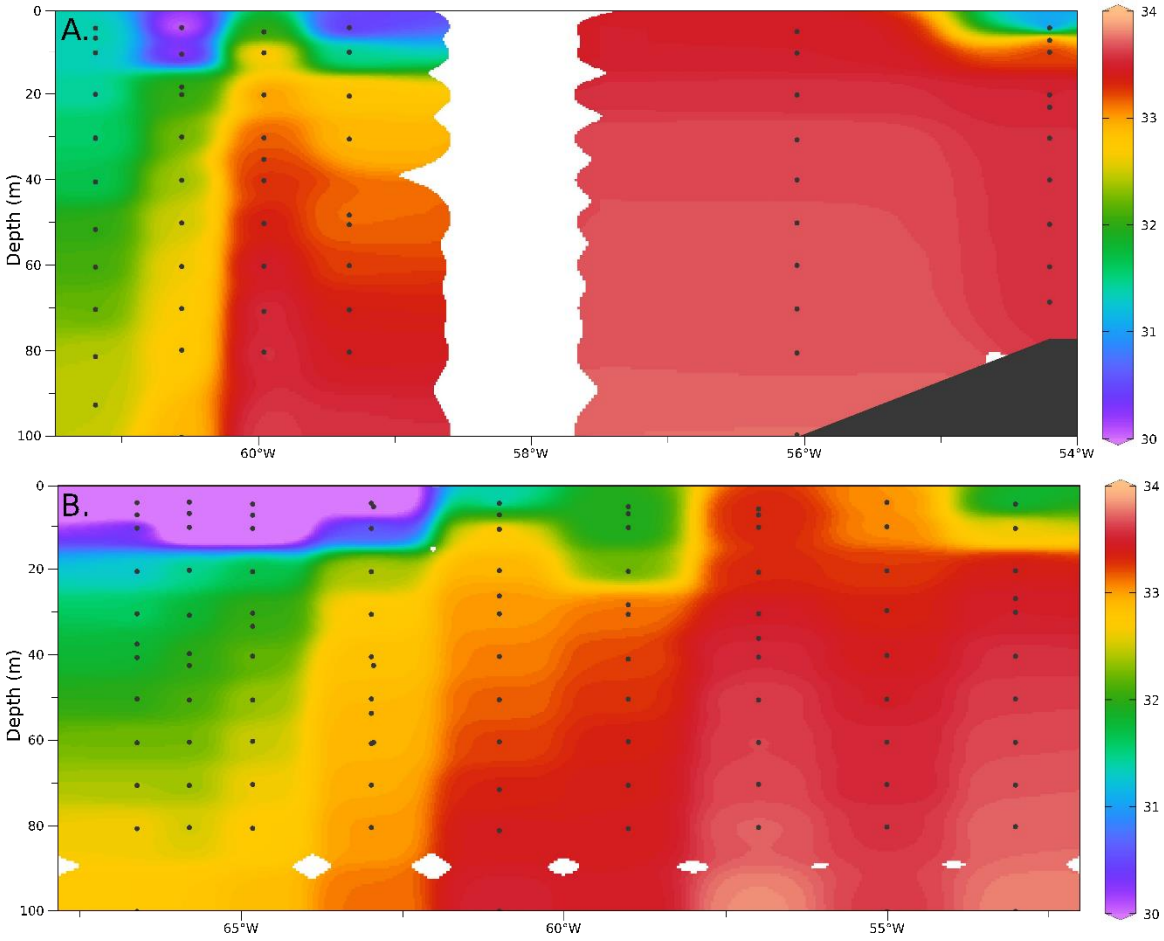

Figure 3.1: Salinity cross sections of A. Transect 1 and B. Transect 2

3.2 CHLOROPHYLL-a

Surface Chlorophyll-a concentrations are shown in Figure 3.3. Chlorophyll-a is low except in the northern Nares Strait, with a particularly large bloom near Petermann Glacier, as well as in Jones Sound, and the western side of Transect 1. Salinity and

temperature data suggest upwelling at the mouth of Jones sound (Figure B.9), coincident with higher NO_3^- and higher chlorophyll-a.

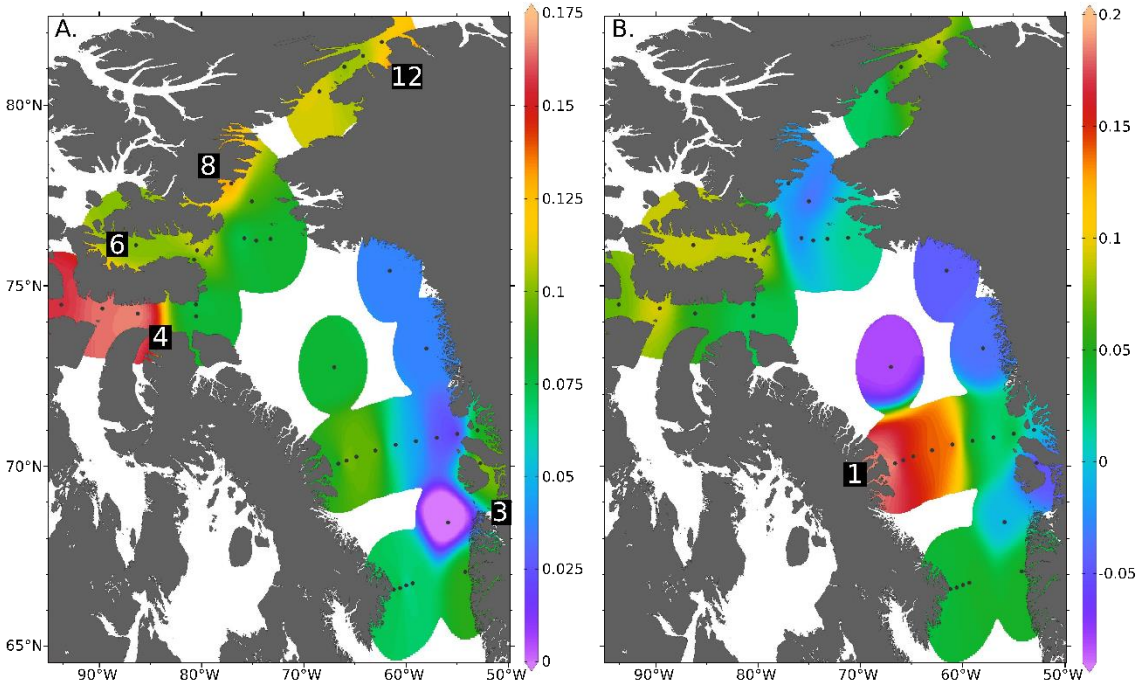

Figure 3.2: A. Fraction of freshwater and B. fraction of sea ice melt in surface water, determined as described in Section 2.3. 1- Clyde River, 3 – Jakobshavn Glacier, 4 – Lancaster Sound, 6 – Jones Sound, 8 – Talbot Inlet, 12 – Petermann Glacier.

3.3 NITRATE CONCENTRATION IN THE ECAA

Nitrate was near zero in all surface waters, except for the eastern and western ends of the Davis Strait (Transect 1 in Figure 2.1, Figure 3.4). At these stations, the $\delta^{15}N$ of NO_3^- was lower in the east, where high chlorophyll-a was also observed, and higher in the west (Figure 3.1). Nitrate accumulated in Jones Sound surface mixed layer (0-1.25 µM), which was likely due to the upwelling of nutrient-rich water. Additionally, riverine input could also be a small source of NO_3^- to this area, as the two rivers sampled in this location, RISG and RIESC, had 3µM NO_3^-. Nitrate was generally completely consumed in the mixed layer (upper 10 m) within the study area and increased with depth to up to

~15 µM at 100 m depth (Figure 3.5). The concentration of NO_3^- in riverine samples was highly variable, ranging from 0.44 to 46.57 µM, as shown in Table 3.1. Nitrite was under 0.2 µM in all samples, both riverine and marine, expect for RI6.1, which had 1.4 µM NO_2^-.

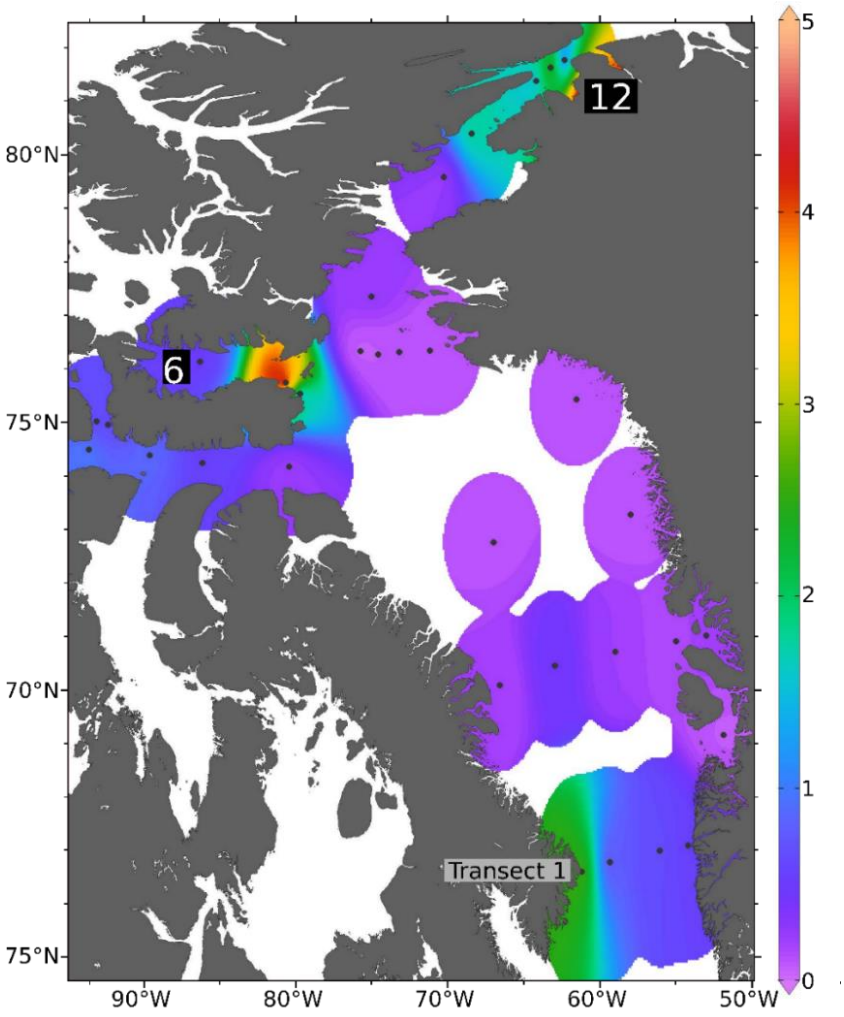

Figure 3.3: Surface chlorophyll-a, regions with blooms at Petermann Glacier (12), Jones Sound (6), and Western Transect 1

High variability was also observed in rivers which are adjacent to one another, such as RI6.1 and ESG. This suggests that the sources of nitrogen in these rivers greatly vary depending on watershed characteristics and microbial metabolisms as suggested by (Kaiser et al., 2017), even within small spatial scales.

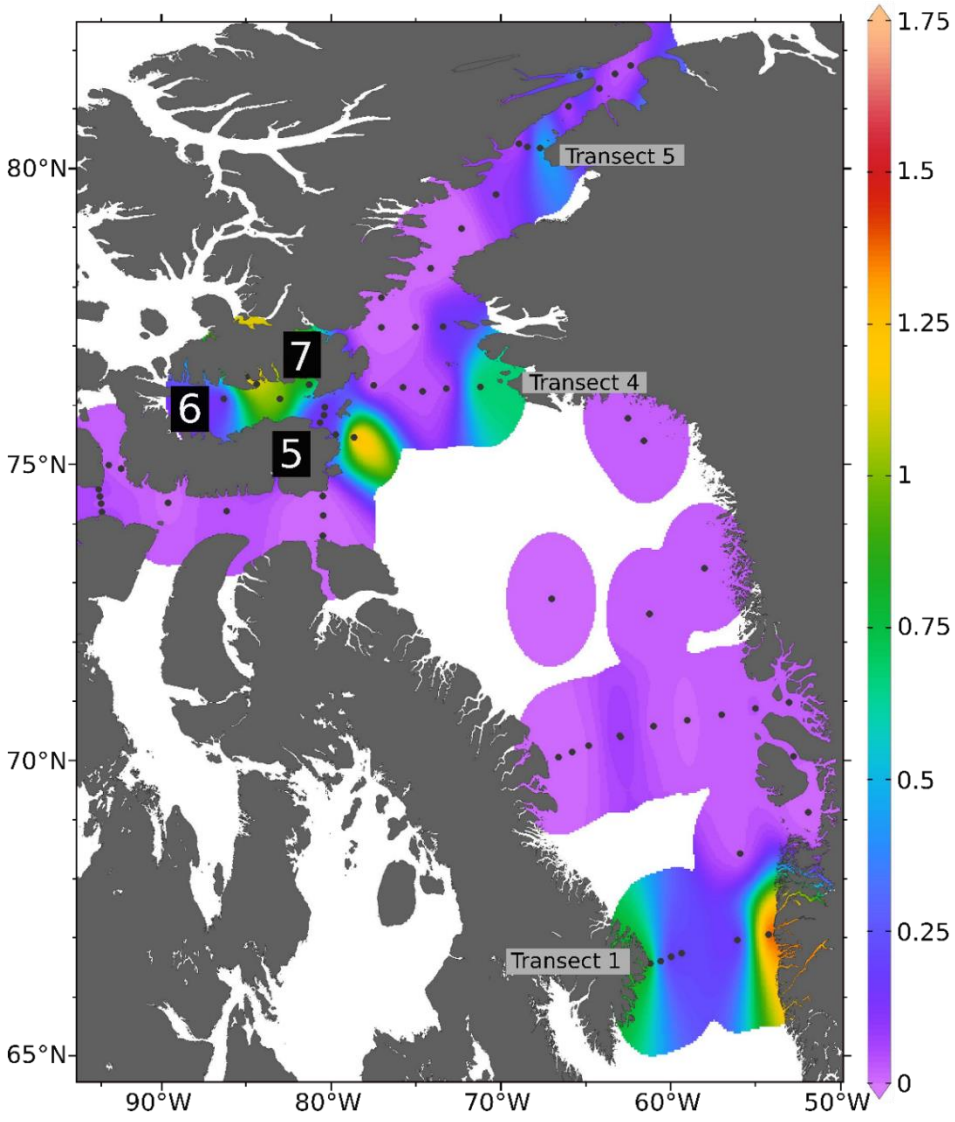

Figure 3.4: NO_3^- (µM) distribution in the surface of the study area. Regions with measurable NO_3^- are labeled as in Figure 2.1.

$\delta^{15}N$ and $\delta^{18}O$ of NO_3^- in freshwater samples are provided in Table 3.1. The isotopic composition of NO_3^- in the rivers was not uniform, further indicating distinct NO_3^- sources in Arctic rivers. The lowest $\delta^{15}N$ of NO_3^- (0.71‰) was observed at RISG. The highest $\delta^{15}N$ of NO_3^- (10.3 ‰) was observed at ESG which was adjacent to a Eugenie Glacier's glacial moraine, and to RI6.1 ($\delta^{15}N$ of NO_3^- of 10.03‰). RI6.1 was about 20-30 meters wide. In contrast, ESG was a river running through a crevasse

adjacent to Eugenie Glacier, and was only ~ 1 meter wide. ESG and RI6.1 were drastically different with respect to their $\delta^{18}O$ of NO_3^-, which was -2.73 ‰ in RI6.1 and 48.7 ‰ in ESG.

High variation was also observed between RIESC and RISG, both of which are west of Grise Fjord. RISG was around 5 meters wide and ~0.5 meters deep, while RIESC was roughly 20 meters wide and 1-2 meters deep. Additionally, RIESC was more inland than RISG. RISG and RIESC had similar NO_3^- concentrations, but the $\delta^{15}N$ of NO_3^- was almost 2‰ higher at RIESC than RISG. Furthermore, the $\delta^{18}O$ of NO_3^- at RIESC was nearly 4.5 times lower than that at RISG. Conversely, two other stations in similar areas, RIDIW and RIDIW-N had very different concentrations of NO_3^-, but similar isotopic signatures.

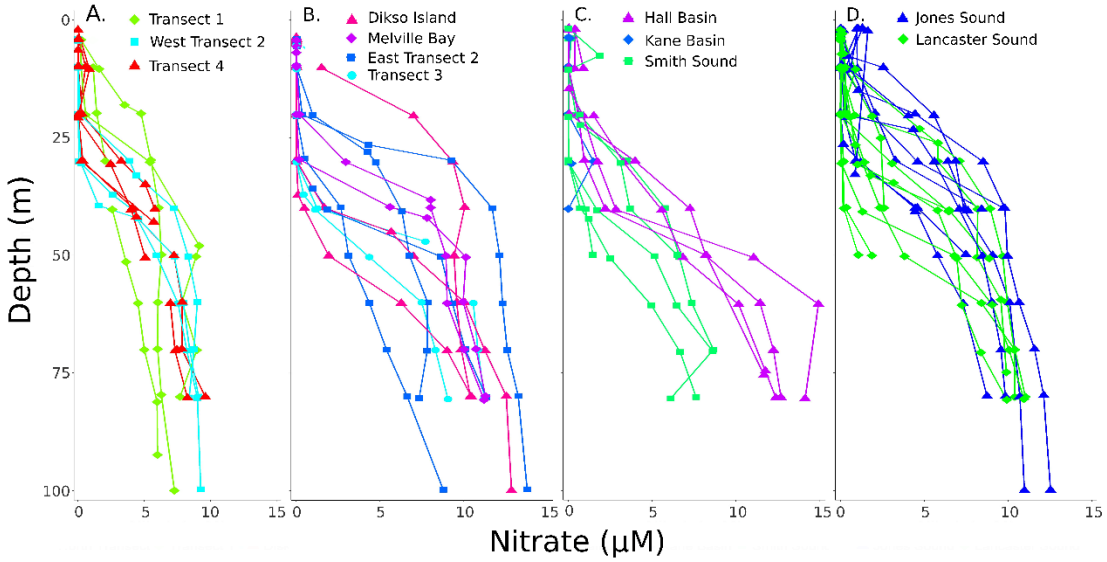

Figure 3.5: Nitrate depth profiles for A. Western Baffin Bay B. Eastern Baffin Bay C. Nares Strait and D. Jones and Lancaster Sounds

Our simple isotopic mass balance model allowed us to better understand the sources of NO_3^- in glacial rivers. The NO_3^- isotopic composition of our samples fell outside the mixing line for the two end members, i.e., nitrification of permafrost or

atmospheric NH_4^+ and atmospheric deposition of NO_3^- (Figure 3.6). However, the riverine isotopic values were within the boundaries of the mixing and assimilation curves considering the large uncertainties associated with end members isotopic compositions. This indicates that all 3 processes contributed, to some extent, to the $\delta^{15}N$ and $\delta^{18}O$ of NO_3^- signatures of the river samples.

Table 3.1: Concentration and $\delta^{15}N$ and $\delta^{18}O$ of NO_3^- and DON, as well as $\Delta(15,18)$ of NO_3^- in river samples.

STATION	$[NO_3^-]$	$\delta^{15}N\text{-}NO_3^-$	$\delta^{18}O\text{-}NO_3^-$	$\Delta(15,18)$	[DON]	$\delta^{15}N\text{-}DON$
RIDIW	20.41	4.36	-9.30	13.65	1.61	
RIDIE	1.29	3.43	17.73	-14.30	0.54	
RICP	4.10	2.93	-7.53	10.46	2.24	
RIDIW-N	46.57	4.77	-9.58	14.35	0.99	
RISG	2.73	0.71	-1.40	2.11	3.07	5.84
RIESC	3.30	2.59	-6.27	8.86	1.80	
RI6.1	11.03	10.03	-2.73	12.76	0.00	
ESG	0.44	10.32	48.72	-38.40	4.89	7.15
RI135	3.47	6.60	7.28	-0.68	0.16	
RIEE	2.70	4.84	10.26	-5.42	1.53	
RIHI	4.65	5.27	-0.80	6.07	1.41	

Additionally, we used this steady-state isotopic model to reproduce the deviation from the $^{18}\varepsilon:^{15}\varepsilon$ ratio of ~1 observed for pure NO_3^- assimilation (Granger et al., 2004) for our riverine samples, i.e., the difference between NO_3^- $\delta^{15}N$ and $\delta^{18}O$, $\Delta(15,18)$ (Rafter et al., 2013). Both scenarios (45% and 30% recycled production) were able to reproduce the full range of observed $\Delta(15,18)$ (Appendix A).

3.4 DON DISTRIBUTION AND $\delta^{15}N$ IN THE ECAA

The surface distribution of DON concentrations and the $\delta^{15}N$ of DON are shown in Figure 3.7. DON concentrations were highly variable but had similar values between regions, ranging from 3.2 to 6.1 μmol N L^{-1} in Baffin Bay and 3.2 to 6.0 μmol N L^{-1} in

the Nares Strait. Lancaster Sound and Jones Sound had lower DON concentrations, ranging from 2.1 to 5.7 μmol N L^{-1}.

In the upper 10 meters of the water column [DON] appeared to decrease at lower salinities (Figure 3.8). This indicated a low [DON] freshwater end member, which corroborated with our direct riverine measurements of [DON]. [DON] in riverine samples were moderate-to-low, even when NO_3^- was high. Yet, no clear relationship between [DON] and freshwater input was observed in Jones Sounds, where freshwater inputs were relatively high (Figure 3.2A). The relationship of DON concentration and $\delta^{15}N$ with depth was variable and often constrained to the upper 40 m due to analytical limitations associated with measuring samples with high concentrations of NO_3^- at depth. Concentration and $\delta^{15}N$ of DON increased with depth in Transects 1 & 2, Lancaster Sound, and in some areas near Disko Island (Appendix Figure B.1, B.2, B.6). DON trends with depth in the Nares Strait were variable. Some of the more southern sections had increased DON at depth with a slightly lower isotopic signal, other parts did not show a significant change in isotopic composition, and others increased slightly in both $\delta^{15}N$ and DON. These higher [DON] observed for the eastern sections of both transects are likely caused by Ekman-driven upwelling.

In two areas of higher chlorophyll-a, the Northern Nares Strait and Western Transect 1, [DON] and $\delta^{15}N$-DON were correlated with chlorophyll-a in the surface mixed layer. Higher chlorophyll-a was positively correlated with lower [DON] (Pearson p-value = 0.04, Spearman p-value = 0.02, ρ= -1; Figure 3.9). Additionally, in these regions lower ln([DON]) was correlated with a higher $\delta^{15}N$-DON (Pearson p-value = 0.10, Spearman p-value = 0.02, ρ= -1; Figure 3.10). These trends were not observed in

Jones Sound, where high chlorophyll was also observed. No relationships were observed between [DON], $\delta^{15}N$ of DON and the fraction of freshwater in Northern Nares Strait and Western transect 1, precluding a significant source of low [DON] and elevated $\delta^{15}N$ DON from rivers at these locations.

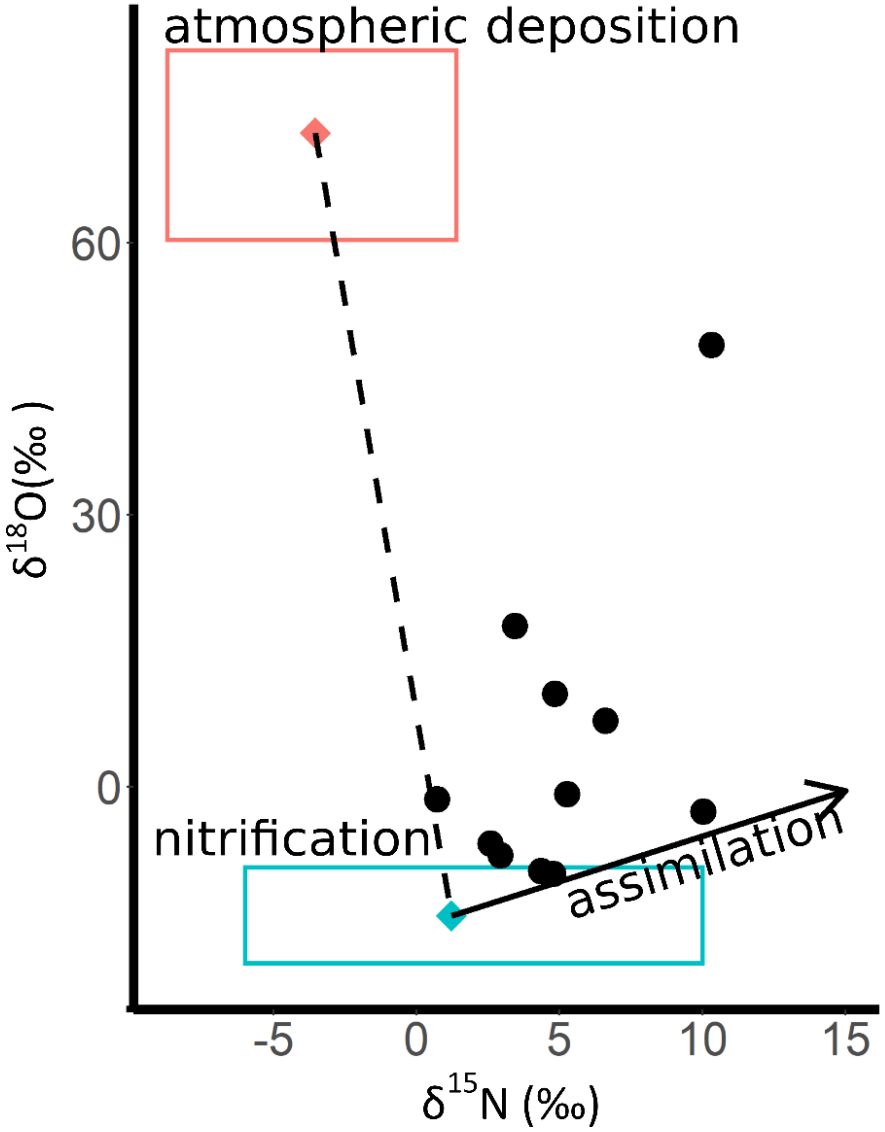

Figure 3.6: $\delta^{18}O$ vs $\delta^{15}N$ of riverine samples, with mixing between nitrification of NH_4^+ (blue box) and atmospheric deposition (pink box) marked by the dashed line. The ε^{18}: ε^{15} of assimilation (~1) is noted with the solid black arrow.

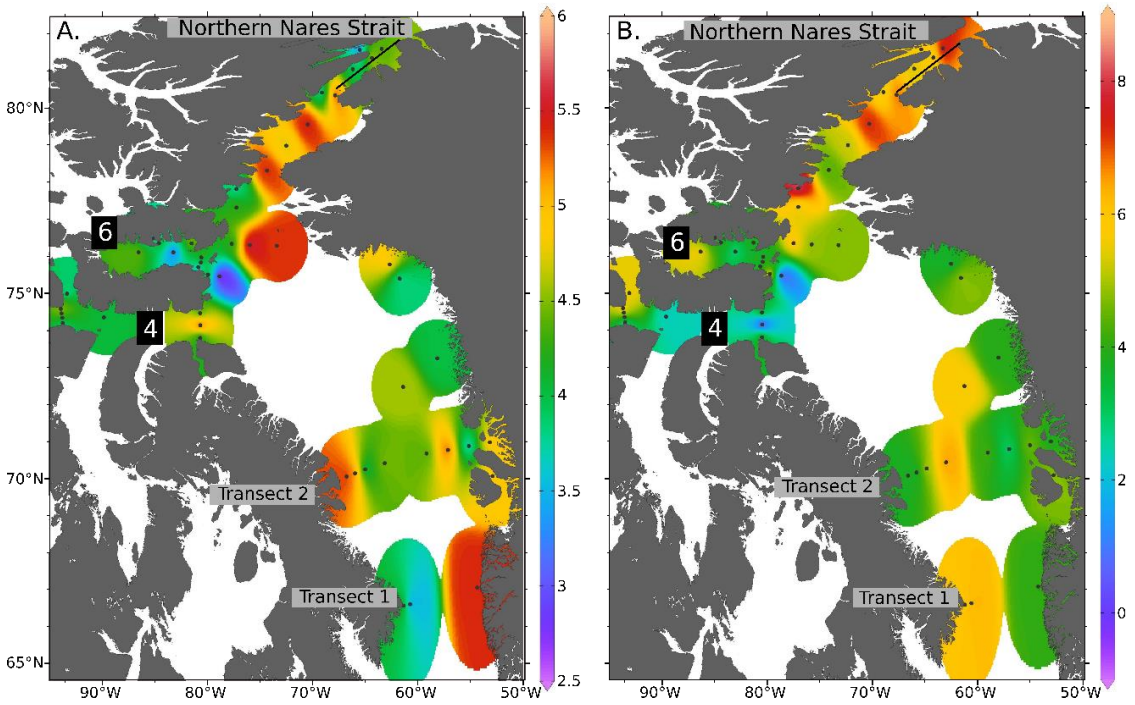

Figure 3.7**:** A. [DON] (µM N L^{-1}) and B. $\delta^{15}N$ of DON in the surface water. Transects 1, 2, and Northern Nares Strait are denoted with black text. Lancaster (4) and Jones (6) Sounds are also labeled.

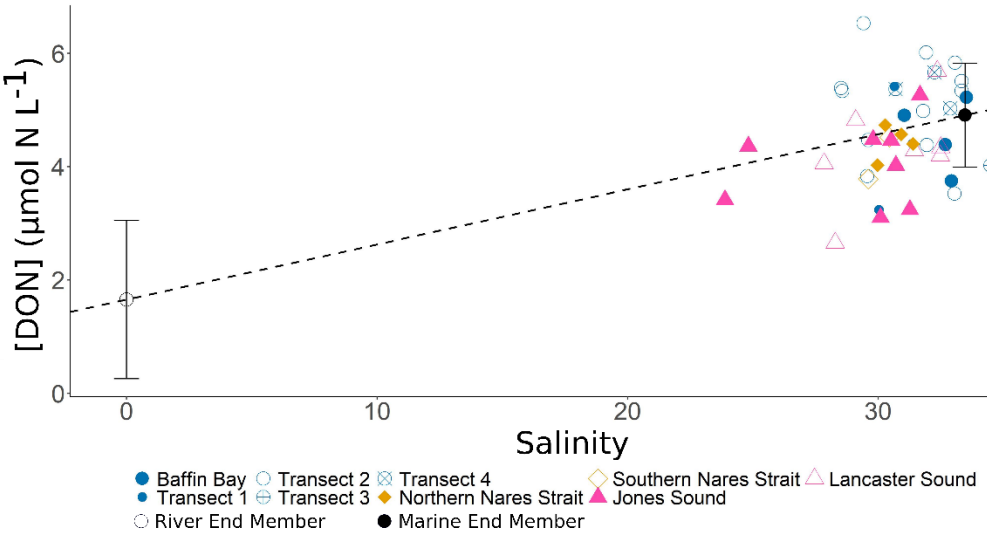

Figure 3.8: [DON] (µM N L^{-1}) in the upper 10 meters of the water column vs salinity. Color indicates close geographic proximity: Blue samples are within Baffin Bay, orange in Nares Strait, pink are in sounds to the east of Baffin Bay. Riverine (hollow) and marine (solid) end members are marked with black dots with solid lines representing standard deviation in our estimates. The dashed line represents mixing between the two end members. Standard deviation < 0.5 for [DON].

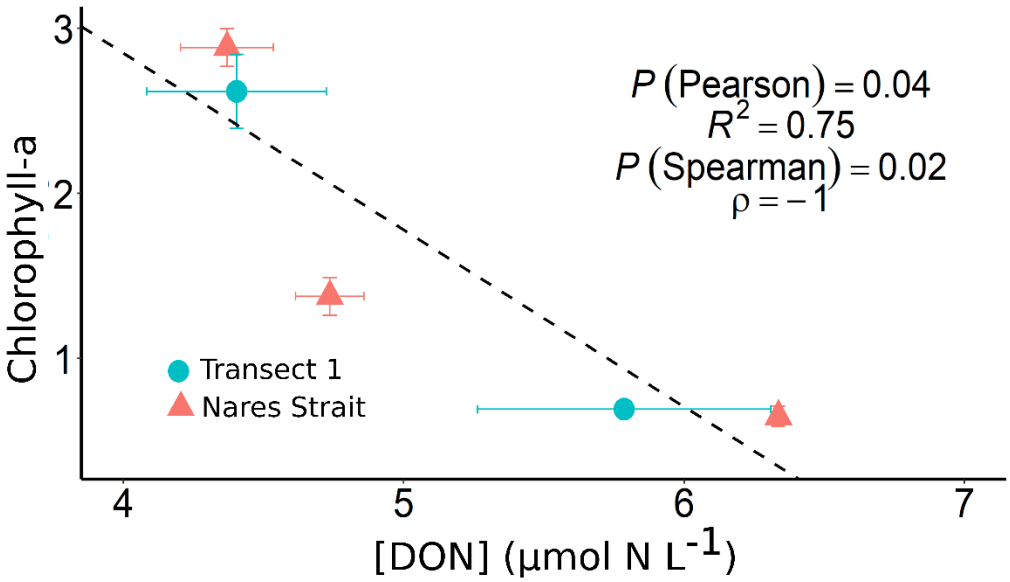

Figure 3.9**:** [DON] (µM N L^{-1}) in the northern Nares Strait (north of 80°N) (comprising Hall Basin and Kennedy Channel) and western Transect 1, against chlorophyll-a. P, R^2 and ρ were determined using both Pearson's and Spearman's rank correlation.

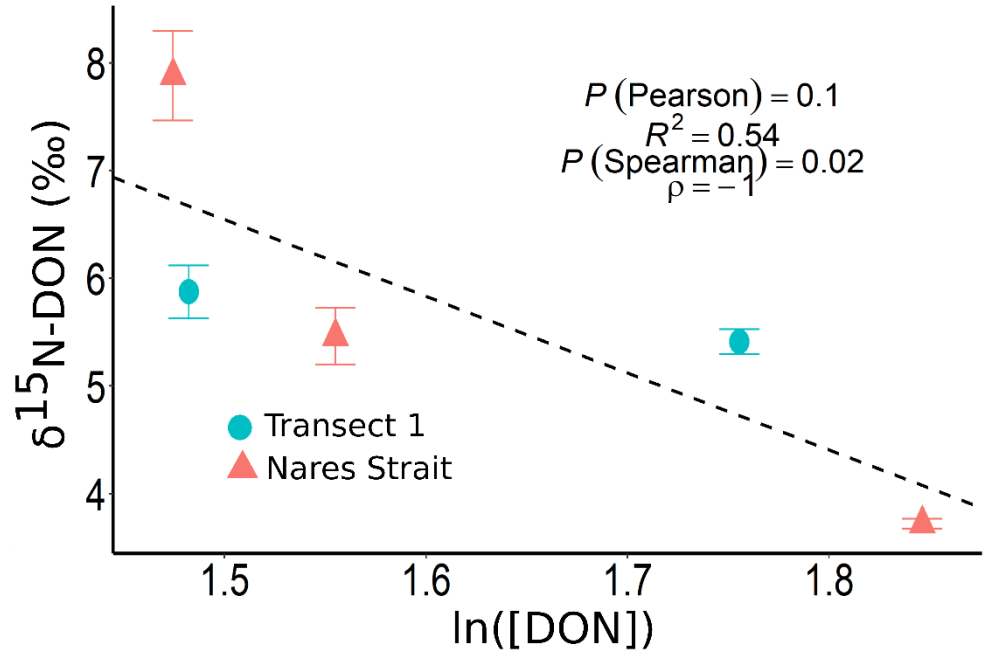

Figure 3.10: ln(DON) vs $\delta^{15}N$ of DON in the northern Nares Strait (north of 80°N) and western Transect 1, R^2 and ρ determined via both Pearson's and Spearman's rank correlation.

CHAPTER 4

DISCUSSION

4.1 NITRATE IN THE ECAA

Nitrate was, on average, zero in the surface mixed layer (upper 10 m depth), though some surface stations had over 1 µM NO_3^- (Figure 3.4). Though some of the glacial rivers sampled had upwards of 10 µM NO_3^-, these elevated concentrations were not observed in coastal marine waters. This indicates that NO_3^- from the rivers is rapidly consumed along the coasts. Previous studies of riverine nutrients in the Arctic have similarly found that riverine NO_3^- delivered into coastal Arctic waters is rapidly consumed nearshore (Emmerton et al., 2008; Tremblay et al., 2014; Tremblay et al., 2015). Riverine nutrient input can increase productivity locally in some near-shore regions, but this only represents a relatively minor fraction of net marine primary productivity in the Arctic (Tremblay et al., 2015). While few blooms were identified through discrete chlorophyll-a sampling, satellite data for July and August 2019 in this region show higher chlorophyll-a and primary productivity nearshore (Appendix B.7 and B.8).

The concentration and isotopic composition of riverine NO_3^- were highly variable spatially, indicating distinct production and consumption processes. We considered two main sources of NO_3^- in rivers, atmospheric deposition or nitrification of NH_4^+ from either permafrost or atmospheric deposition. Some rivers with low [NO_3^-] had particularly high $\delta^{18}O$, up to 48‰, suggesting input from atmospheric deposition. The

$\delta^{18}O$ of NO_3^- from atmospheric deposition in the summer reflects the $\delta^{18}O$ of the sources of O, which are ozone (O_3) and hydroxyl radicals (OH). O_3 has a higher $\delta^{18}O$ (90-122‰; (Johnston & Thiemens, 1997; Krankowsky et al., 1995), while OH is usually below zero (Hastings et al., 2004). NO_3^- receives two O atoms from O_3, and one from OH, therefore the $\delta^{18}O$ of NO_3^- from atmospheric deposition should be elevated (65.2 to 79.6‰; Hastings et al., 2004) due to the predominant influence of O_3. Additionally, other rivers had a low $\delta^{18}O$, which could be due to nitrification of NH_4^+. Because water donates two oxygen atoms during nitrification, the $\delta^{18}O$ of the ambient water can be imprinted onto the NO_3^- produced (Buchwald et al., 2010; Casciotti et al., 2010). Freshwater in high latitude systems has a lower $\delta^{18}O$ (-12 to -22‰; Arendt et al., 2016; Wynn et al., 2007) than freshwater elsewhere, and therefore the low $\delta^{18}O$ of NO_3^- observed in river waters here could be due to the low $\delta^{18}O$ of the freshwater during nitrification.

To determine the significance of these end members we applied our steady-state isotopic model described in Chapter 2.4 and Appendix A, and were able to reproduce the range of observed $\Delta(15,18)$ in riverine samples (Figure A.l). The NO_3^- isotopic signatures (both $\delta^{15}N$ and $\delta^{18}O$) suggested that mixing between atmospheric NO_3^- and nitrified NH_4^+ alone could not account for the observed $\delta^{15}N$ and $\delta^{18}O$. However, including NO_3^- assimilation allowed explaining the observed dual NO_3^- isotopic values (solid arrow in Figure 3.6). This requirement for NO_3^- removal by assimilation is corroborated by previous studies, which have observed the uptake of NO_3^- by phytoplankton in Arctic rivers (Beaton et al., 2017; Snyder & Bowden, 2014). Our isotopic model also suggests that the majority of our data appear to be more influenced by the input of microbially-derived (nitrified) NO_3^- rather than atmospheric NO_3^-. This indicates that nitrification is

putatively an important source of bioavailable N to Arctic rivers. Arctic permafrost is known to have a large quantity of NH_4^+ (Fouché et al., 2020), and contact with permafrost can influence chemical composition of rivers (Frey et al., 2007; Frey & McClelland, 2009; Heikoop et al., 2015; Vonk et al., 2015). Additionally, NH_4^+ can be found in atmospheric deposition in similar proportions to atmospheric NO_3^- (Clark et al., 2020; Fouché et al., 2020). Moreover, NO_3^- input from atmospheric deposition appears to be temporally variable. In the Canadian Arctic, atmospheric deposition can be a dominant source of NO_3^- in rivers during the early melt season, which is from early June to mid-July. Rivers in this study were sampled after this melt season, during which remineralization or nitrification takes over as the dominant source of NO_3^- (Louiseize et al., 2014).

Though nitrification of permafrost or atmospheric deposition NH_4^+ was the predominant source of NO_3^-, some rivers had significantly higher NO_3^- concentrations than others, even when they were geographically close to one another. For instance, rivers RI6.1 and ESG were adjacent, but ESG has the lowest $\Delta(15,18)$ (-38.40‰) and RI6.1 had the 3rd highest $\Delta(15,18)$ (12.76‰). We attribute this extreme variability to different landscape features associated with these rivers. ESG was running directly through a glacier, while RI6.1 was next to a glacial moraine containing significant terrestrial material. Therefore, ESG was likely in more direct contact with the glacial end member than RI6.1—this could affect the chemical composition of the two rivers. However, in order to more quantitatively analyze NO_3^- cycling in these rivers, the end members need to be better constrained in future studies.

4.2 DON in the ECAA

Several factors control primary productivity in the Arctic, such as nitrogen, iron and light availability (Tremblay et al., 2015). Ongoing Arctic sea ice loss is expected to increase light availability, and drastically impact primary productivity and, consequently biological CO_2 intake (Arrigo, 2007; Frey, 2018; Hill et al., 2018). Furthermore, river discharges from Arctic watersheds are steadily increasing in response to changes in the North Atlantic Oscillation and global mean surface air temperature (McClelland et al., 2016; Peterson et al., 2002; Rood et al., 2017). These rivers transport massive quantities of dissolved and particulate inorganic and organic nitrogen, sustaining primary productivity in coastal waters (Letscher, et al., 2013; McClelland et al., 2016; Thibodeau et al., 2017).

In this study, NO_3^- concentrations were extremely low or zero in the ECAA surface waters, which is consistent with N being the limiting nutrient in Arctic regions (Figure 3.4). However, DON accumulated to concentrations up to 6.10 μmol N L^{-1} in surface waters (Figure 3.7A) and could thus sustain primary productivity, if a significant fraction of that DON is labile. However, the lability of the DON pool was not directly analyzed in this study. At depth, DON concentration and isotopic composition was variable. Most studies have observed a decrease in [DON] at depth (eg. Hopkinson et al., 1997; Knapp et al., 2018; Torres-Valdés et al., 2009), though one study by Maita & Yanada (1990) observed an increase in one nearshore station. The differences observed in this study could be due to local variations in DON sources. Previous studies have found that the $\delta^{15}N$ DON can reflect the $\delta^{15}N$ of the new N source (Knapp et al., 2018). In short, DON produced from a low $\delta^{15}N$ source, such as newly nitrified NO_3^- from N_2 fixation,

can have a similarly low $\delta^{15}N$ DON. In samples where we were able to measure both $\delta^{15}N$ of NO_3^- and DON, the $\delta^{15}N$ of DON was on average ~4 ‰ lower than that of NO_3^-. This is similar to what was observed in Knapp et al. (2018), where DON accumulated in the subsurface bracketed the $\delta^{15}N$ of subsurface NO_3^- by ±3‰. Additionally, the lack of variation in DON isotopic composition observed in some areas could suggest recalcitrant DON (Bourbonnais et al., 2009; Knapp et al., 2005).

Previous studies suggest that rivers are generally a significant source of bioavailable DON. For instance, Lobbes et al. (2000) reported an average [DON] of 12 µM for 12 Russian rivers. Conversely, Thibodeau et al. (2017) measured DON concentrations ranging between 13.9-21.8 µM in the Siberian Arctic. These studies found that up to 70% of the terrigenous DON delivered by Arctic rivers was consumed within the shelf waters of the western and Eurasian Arctic (Letscher et al., 2013; Thibodeau et al., 2017). Our results contrast with findings from other Arctic regions, such as the Siberian and Western Arctic (Dittmar et al., 2001; Holmes et al., 2012; Lobbes et al., 2000; Thibodeau et al., 2017). Glacial rivers measured in this study generally had relatively high NO_3^- but were mostly depleted in DON (up to 4.89 µmol N L^{-1}). Our study thus suggest that glacial rivers in the ECAA could act to dilute the surface waters DON pool. Overall, salinity in the upper 10 meters was negatively correlated with lower [DON], though this correlation was not significant (Figure 3.8). This could be due to simultaneous production and consumption of DON complicating the relationship between DON and salinity. Nonetheless, this general trend corroborates the observations of low DON in ECAA rivers. Glacial rivers' inputs could thus further stratify the water column, inhibiting vertical exchange with nutrient-rich deep waters, potentially decreasing

primary productivity in the region if DIN is also low. These varying DON concentrations observed between studies are likely related to the amount of glacial coverage, as the ECAA has significantly higher glacial coverage than the western and Eurasian Arctic (Pfeffer et al., 2014).

Notably, Western Lancaster Sound, where a particularly high fraction of freshwater was observed, is fed by several rivers which we directly measured, as well as run off from the Devon Ice Cap. The rivers RIDIW, RIDIW-N, and RICP all drain into western Lancaster Sound and had low [DON], ranging from 0.99 - 2.24 µmol N L^{-1}. This is a lower concentration than the surface ocean [DON] of this region, which is ~4 µmol N L^{-1}. Additionally, prior studies have found that [DON] in run off from the Leverett Glacier in the Greenland ice sheet ranges from 0.1-6.3 µM, with a mean of 1.7 µM (Wadham et al., 2016). All the [DON] values of rivers in this study fall within this range, though none of these rivers were draining from the Greenland Ice Sheet. Thus, our direct measurements of [DON] in glacially fed rivers corroborate dilution of the marine DON pool by glacial riverine freshwater. Deviations from a pure mixing line in Figure 3.8 strongly suggest that competing sources or transformations are affecting the DON pool, e.g., inputs from freshwater and buoyancy or Ekman-driven upwellings and *in-situ* production/consumption by phytoplankton assemblages in the mixed surface waters (Cape et al., 2019; Thibodeau et al., 2017).

The concentration of in glacial rivers greatly. For example, on the Greenland Ice Sheet and the Leverett Glacier, which is adjacent to eastern Transect 1 in this study, previous studies reported a range from 5.1-14 µM for DON in the surface ice, while DON in basal ice and summer ice melt was on average about 12 µM and 3.0 µM, respectively

(Holland et al., 2019; Wadham et al., 2016). The higher DON values in both locations were attributed to the presence of debris or microbial production of DON. However, other studies reported near zero DON concentration in supraglacial streams, cryoconite melt water, snow, and short ice cores (Holland et al., 2019; Telling et al., 2012; Wadham et al., 2016). In contrast, runoff from the Leverett Glacier had an average DON concentration of 1.7 µM, with a maximum of 6.3 µM (Wadham et al., 2016). This average value is low relative to the average [DON] of the adjacent marine waters (5.55 µmol N L^{-1}). Thus, the low [DON] seen in river samples in this study could be characteristic of glacial melt that has not mixed with high DON basal ice or debris.

Our isotopic model for riverine NO_3^- suggested that nitrified NH_4^+ is a significant source of NO_3^- in most rivers observed in this study. However, rivers with more contact between the sources of organic matter such as permafrost and debris are typically DON-rich (Fouché et al., 2020; Frey et al., 2007; Frey & McClelland, 2009; Wadham et al., 2016). These two statements may be reconciled in the future by better constraining the isotopic composition ($\delta^{15}N$) of permafrost DON as well as improvements into the methodology used for DON isotopic analysis, at high NO_3^- concentrations. For example, Frey & McClelland (2007) found that there was greater remineralization of organic nitrogen in the permafrost of Alaskan watersheds compared to West Siberian watersheds. DON remineralization taking place within the permafrost could imprint an isotopic signal on riverine DON as they mix. Current analytical methods require DON to equal at least 50% TDN, and therefore the DON could not be analyzed in most of our riverine samples. However, though the concentrations were too low relative to NO_3^-, almost all riverine DON concentrations were well within the detection limits for isotopic analysis if DON

could be isolated from DIN. Therefore, improvements to the analytical methods for measuring stable isotopes of DON (e.g., capability to remove DIN prior to DON analysis) could elucidate the contribution of permafrost in delivering DON to glacially fed rivers.

Though rivers in this region were not a significant source of DON, another potential source of DON in the Arctic is sea ice melt. Similar to surface ice in some glaciers, sea ice can have higher concentration of DON, as observed in the Antarctic (Dall'Osto et al., 2017; Fripiat et al., 2014). Fripiat et al. (2014) suggested high DON was released by microbial communities within the sea ice following NO_3^- assimilation. However, no significant correlation was observed between sea ice melt and DON in this study. Higher resolution sea ice melt and DON datasets, as well as direct measurements of DON in Arctic sea ice could help explore this potential contribution.

Because [DON] was <50% [TDN] in all but 2 of the rivers, we could not measure the δ^{15}N-DON of most of the rivers. However, both RISG and ESG had slightly elevated δ^{15}N-DON (5.84‰ and 7.15‰, respectively). Prior studies have observed low δ^{15}N-DON in rivers and streams, at around -4 to 2 ‰ (Thibodeau et al., 2017; Ye et al., 2018). These values have been attributed to N sources from atmospheric deposition, aquatic and/or terrestrial N_2 fixation, or plant litter decomposition. Assuming DON sources in these rivers would have similar δ^{15}N to this range, the values observed here could be considered elevated, and may indicate kinetic isotope fractionation during consumption or a source of recalcitrant DON with a particularly high δ^{15}N (e.g., Bourbonnais et al., 2009; Knapp et al., 2005). DON consumption will preferentially utilize the lighter isotopes, elevating the δ^{15}N-DON of the remaining pool (Knapp et al., 2018). Identifying the sources and lability of DON in these rivers, and the microbial processes involved

could provide further insights on how changes in river discharge and glacial coverage will affect DON supply. Overall, our data shows significant variability in DON concentrations and isotopic composition in ECAA rivers. Therefore, special caution should be used when extrapolating these measurements to the global Arctic N budget, as the sources and processes determining [DON] and isotopic signatures are not homogenous across Arctic rivers.

4.3 ALGAL CONSUMPTION OF DON

DON consumption was identified at two main regions in the study area. One of the signals of DON consumption is the enrichment of the DON pool (Knapp et al., 2018). During consumption, ^{14}N is preferentially taken up, resulting in an increase in the $\delta^{15}N$ of the substrate in surface waters. We observed a negative relationship between chlorophyll-a and DON concentrations in both the northern segment of the Nares Strait and the western half of Transect 1 (Pearson p-value = 0.04, Spearman p-value = 0.02, ρ= -1; Figure 3.9). Additionally, in Figure 3.10, higher [DON] is negatively correlated with $\delta^{15}N$ (Pearson p-value = 0.10, Spearman p-value = 0.02, ρ= -1). Our derived isotope effect of -6.9‰ using a closed-system Rayleigh model (Figure 3.10), is comparable to previously measured isotope effects of DON consumption of -5.5‰ (Knapp et al., 2018).

We observe that higher chlorophyll-a is correlated with lower [DON], which contrasts with the relationship found by Knapp et al. (2018). Knapp et al. (2018) observed a positive correlation between surface ocean chlorophyll-a and DON concentrations in the eastern tropical South Pacific, consistent with a photosynthetic source for DON. Conversely, nutrient concentration has been shown to decrease as chlorophyll-a increases due to nutrient uptake by phytoplankton in incubation studies

(Buapet et al., 2008; Cruz et al., 2006), and a similar inverse relationship has been observed between DON and chlorophyll-a in lakes (Berman, 1997). We posit that the low DON associated with high chlorophyll-a observed here is the result of net DON uptake by phytoplankton.

Though [DON] remains at around 4-5 μM N L^{-1} in the surface waters throughout most of the study region and NO_3^- is near or at zero, we do not observe a distinct consumption signal at other stations. There are several possibilities to explain this. First, any correlation between [DON] and chlorophyll-a is likely hindered by the low spatial resolution of available chlorophyll-a measurements, though satellite data corroborates our observations of mostly low chlorophyll-a in Baffin Bay (Figure B.7). Second, DON could be recalcitrant in some regions, and therefore would not support a phytoplankton bloom. Dittmar et al. (2001) found that DON in the Siberian Arctic in brackish mixing zones was relatively recalcitrant. Third, DON cycling is likely complex and highly dynamic, with simultaneous consumption, production, and regeneration decoupled in space and time. For example, new DON produced from inorganic N will tend to be more labile, which can then be rapidly consumed (Knapp et al., 2005, 2018). These processes would complicate the relationship between chlorophyll-a and DON.

CHAPTER 5

CONCLUSION

Nitrogen is a limiting nutrient in the ECAA, but its cycling and dynamic are not well constrained, particularly with regards to DON. As river discharges are projected to increase under a warmer climate, it is critical to better understand the role of glacial rivers in delivering nitrogen to this climate sensitive region.

NO_3^- was the dominant dissolved nitrogen species in rivers. Our stable isotopic data suggests that a significant fraction of this NO_3^- was assimilated in the river and/or rapidly consumed near shore. Thus, while increased river discharge may increase riverine NO_3^- flux, the impact on primary productivity may be limited to coastal regions (Tank et al., 2012; Tremblay et al., 2015).

We used a steady-state isotopic box model to apportion the sources of NO_3^- in rivers. Our model suggested that NO_3^- assimilation in addition to mixing between inputs from atmospheric deposition and nitrified NH_4^+ is needed to explain the observed $\delta^{15}N$ and $\delta^{18}O$ of NO_3^- in rivers. NO_3^- putatively derived from the nitrification of permafrost or atmospheric NH_4^+ was found to be a main source of NO_3^- in most rivers, while only few rivers (e.g., ESG) had significant input of NO_3^- from atmospheric deposition.

DON concentrations were relatively low in rivers (less than 4.89μM N L^{-1}). Unlike relationships observed for coastal waters adjacent to major Arctic rivers (Letscher et al., 2013; Thibodeau et al., 2017; Tremblay et al., 2002)

we observed that DON concentrations were generally increasing with salinity. We posit that increased riverine discharge in the ECAA may result in increased stratification of the surface ocean and dilution of the ambient DON pool, with potential effect on primary productivity.

We observed evidence for DON consumption (i.e., negative correlations between chlorophyll-a and DON concentrations as well as DON concentration and $\delta^{15}N$) in the northern Nares Strait, as well as western Transect 1. This indicates that DON can fuel primary productivity in the ECAA, although the source of this DON, as well as its composition and lability require further investigation. We estimated an isotope effect for DON consumption of -6.9‰ , which is in line with previous studies (-5.5‰; Knapp et al., 2018).

This study provides a baseline for DON cycling in the ECAA and highlights further areas of research needed to better understand N-cycling in this dynamic region. In particular, end members for permafrost N need to be better constrained to better differentiate the sources of NO_3^- in rivers.

REFERENCES

Ahmed, M. M. M., Else, B. G. T., Capelle, D., Miller, L. A., & Papakyriakou, T. (2020). Underestimation of surface pCO2 and air-sea CO2 fluxes due to freshwater stratification in an Arctic shelf sea, Hudson Bay. *Elementa: Science of the Anthropocene*, *8*(1). https://doi.org/10.1525/elementa.084

Alkire, M. B., Falkner, K. K., Boyd, T., & Macdonald, R. W. (2010a). Sea ice melt and meteoric water distributions in Nares Strait, Baffin Bay, and the Canadian Arctic Archipelago. *Journal of Marine Research*, *68*(6), 767–798. https://doi.org/10.1357/002224010796673867

Alkire, M. B., Falkner, K. K., Boyd, T., & Macdonald, R. W. (2010b). Sea ice melt and meteoric water distributions in Nares Strait, Baffin Bay, and the Canadian Arctic Archipelago. *Journal of Marine Research*, *68*(6), 767–798. https://doi.org/10.1357/002224010796673867

Altabet, M. A. (2001). Nitrogen isotopic evidence for micronutrient control of fractional NO3- utilization in the equatorial Pacific. *Limnology and Oceanography*, *46*(2), 368--380.

Alves, R. J. E., Wanek, W., Zappe, A., Richter, A., Svenning, M. M., Schleper, C., & Urich, T. (2013). Nitrification rates in Arctic soils are associated with functionally distinct populations of ammonia-oxidizing archaea. *The ISME Journal*, *7*(8), 1620–1631. https://doi.org/10.1038/ismej.2013.35

Ansari, A. H., Hodson, A. J., Heaton, T. H. E., Kaiser, J., & Marca-Bell, A. (2013). Stable isotopic evidence for nitrification and denitrification in a High Arctic glacial ecosystem. *Biogeochemistry*, *113*(1–3), 341–357. https://doi.org/10.1007/s10533-012-9761-9

Arendt, C. A., Heikoop, J. M., Newman, B. D., Wilson, C. J., Graham, D. E., Dafflon, B., et al. (2016). Isotopic and Chemical Identification of Hydrological Pathways in a Watershed Underlain by Shallow Discontinuous Permafrost, *2016*, GC43E--1199.

Arrigo, K. (2007). Physical control of primary productivity in Arctic and Antarctic polynyas. *Elsevier Oceanography Series*, *74*, 223–238.

Beaton, A. D., Wadham, J. L., Hawkings, J., Bagshaw, E. A., Lamarche-Gagnon, G., Mowlem, M. C., & Tranter, M. (2017). High-Resolution in Situ Measurement of

Nitrate in Runoff from the Greenland Ice Sheet. *Environmental Science & Technology*, *51*(21), 12518–12527. https://doi.org/10.1021/acs.est.7b03121

Bedard, P., Hillaire-Marcel, C., & Page, P. (1981). 18O modelling of freshwater inputs in Baffin Bay and Canadian Arctic coastal waters. *Nature*, *293*.

Berman, T. (1997). Dissolved organic nitrogen utilization by an Aphanizomenon bloom in Lake Kinneret. *Journal of Plankton Research*, *19*(5), 577–586.

Berman, Tom, & Bronk, D. (2003). Dissolved organic nitrogen: a dynamic participant in aquatic ecosystems. *Aquatic Microbial Ecology*, *31*, 279–305.

Bintanja, R., & Selten, F. M. (2014). Future increases in Arctic precipitation linked to local evaporation and sea-ice retreat. *Nature*, *509*(7501), 479–482. https://doi.org/10.1038/nature13259

Bourbonnais, A., Lehmann, M. F., Waniek, J. J., & Schulz-Bull, D. E. (2009). Nitrate isotope anomalies reflect N2 fixation in the Azores Front region (subtropical NE Atlantic). *Journal of Geophysical Research: Oceans (1978–2012)*, *114*(C3). https://doi.org/10.1029/2007jc004617

Braman, R. S., & Hendrix, S. A. (1989). Nanogram Nitrite and Nitrate Determination in Environmental and Biological Materials by Vanadium(III) Reduction with Chemiluminescence Detection. *Analytical Chemistry*, *61*, 2715–2718.

Bronk, D. H., See, J. H., Bradley, P., & Killberg, L. (2007). DON as a source of bioavailable nitrogen for phytoplankton. *Biogeosciences*, *4*, 283–296.

Buapet, P., Hiranpan, R., Ritchie, R. J., & Prathep, A. (2008). Effect of nutrient inputs on growth, chlorophyll, and tissue nutrient concentration of Ulva reticulata from a tropical habitat. *ScienceAsia*, *34*(2), 245. https://doi.org/10.2306/scienceasia1513-1874.2008.34.245

Buchwald, C., & Casciotti, K. L. (2010). Oxygen isotopic fractionation and exchange during bacterial nitrite oxidation. *Limnology and Oceanography*, *55*(3), 1064–1074. https://doi.org/10.4319/lo.2010.55.3.1064

Buchwald, C., Santoro, A. E., McIlvin, M. R., & Casciotti, K. L. (2012). Oxygen isotopic composition of nitrate and nitrite produced by nitrifying cocultures and natural marine assemblages. *Limnology and Oceanography*, *57*(5), 1361–1375. https://doi.org/10.4319/lo.2012.57.5.1361

Burt, W. J., Westberry, T. K., Behrenfeld, M. J., Zeng, C., Izett, R. W., & Tortell, P. D. (2018). Carbon: Chlorophyll Ratios and Net Primary Productivity of Subarctic Pacific Surface Waters Derived From Autonomous Shipboard Sensors. *Global Biogeochemical Cycles*, *32*(2), 267–288. https://doi.org/10.1002/2017gb005783

Cape, M. R., Straneo, F., Beaird, N., Bundy, R. M., & Charette, M. A. (2019). Nutrient release to oceans from buoyancy-driven upwelling at Greenland tidewater glaciers. *Nature Geoscience*, *12*(1), 34–39. https://doi.org/10.1038/s41561-018-0268-4

Carpenter, E. J., Harvey, H. R., Fry, B., & Capone, D. G. (1997). Biogeochemical tracers of the marine cyanobacterium Trichodesmium. *Deep Sea Research Part I: Oceanographic Research Papers*, *44*(1), 27–38. https://doi.org/10.1016/s0967-0637(96)00091-x

Casciotti, K L, Sigman, D. M., Hastings, M. G., Böhlke, J. K., & Hilkert, A. (2002). Measurement of the Oxygen Isotopic Composition of Nitrate in Seawater and Freshwater Using the Denitrifier Method. *Analytical Chemistry*, *74*(19), 4905–4912. https://doi.org/10.1021/ac020113w

Casciotti, Karen L., McIlvin, M., & Buchwald, C. (2010). Oxygen isotopic exchange and fractionation during bacterial ammonia oxidation. *Limnology and Oceanography*, *55*(2), 753–762. https://doi.org/10.4319/lo.2010.55.2.0753

Clark, S. C., Granger, J., Mastorakis, A., Aguilar-Islas, A., & Hastings, M. G. (2020). An Investigation Into the Origin of Nitrate in Arctic Sea Ice. *Global Biogeochemical Cycles*, *34*(2). https://doi.org/10.1029/2019gb006279

Cruz, F. L.-D. la, Valenzuela-Espinoza, E., Millán-Núñez, R., Trees, C. C., Santamaría-del-Ángel, E., & Núñez-Cebrero, F. (2006). Nutrient uptake, chlorophyll a and carbon fixation by Rhodomonas sp. (Cryptophyceae) cultured at different irradiance and nutrient concentrations. *Aquacultural Engineering*, *35*(1), 51–60. https://doi.org/10.1016/j.aquaeng.2005.08.004

Dall'Osto, M., Ovadnevaite, J., Paglione, M., Beddows, D. C. S., Ceburnis, D., Cree, C., et al. (2017). Antarctic sea ice region as a source of biogenic organic nitrogen in aerosols. *Scientific Reports*, *7*(1), 6047. https://doi.org/10.1038/s41598-017-06188-x

Dalsgaard, T., Stewart, F. J., Thamdrup, B., Brabandere, L. D., Revsbech, N. P., Ulloa, O., et al. (2014). Oxygen at Nanomolar Levels Reversibly Suppresses Process Rates and Gene Expression in Anammox and Denitrification in the Oxygen Minimum Zone off Northern Chile. *MBio*, *5*(6), e01966-14. https://doi.org/10.1128/mbio.01966-14

Dittmar, T., Fitznar, H. P., & Kattner, G. (2001). Origin and biogeochemical cycling of organic nitrogen in the eastern Arctic Ocean as evident from D- and L-amino acids. *Geochimica et Cosmochimica Acta*, *65*(22), 4103--4114.

Emmerton, C. A., Lesack, L. F. W., & Vincent, W. F. (2008). Nutrient and organic matter patterns across the Mackenzie River, estuary and shelf during the seasonal recession of sea-ice. *Journal of Marine Systems*, *74*(3–4), 741–755. https://doi.org/10.1016/j.jmarsys.2007.10.001

Fawcett, S. E., Lomas, M. W., Casey, J. R., Ward, B. B., & Sigman, D. M. (2011). Assimilation of upwelled nitrate by small eukaryotes in the Sargasso Sea. *Nature Geoscience*, *4*(10), 717–722. https://doi.org/10.1038/ngeo1265

Fouché, J., Christiansen, C. T., Lafrenière, M. J., Grogan, P., & Lamoureux, S. F. (2020). Canadian permafrost stores large pools of ammonium and optically distinct dissolved organic matter. *Nature Communications*, *11*(1), 4500. https://doi.org/10.1038/s41467-020-18331-w

Frey, K. (2018). Arctic Ocean Primary Productivity: The Response of Marine Algae to Climate Warming and Sea Ice Decline. *Arctic Report Card 2018], Https://Www. Arctic. Noaa. Gov/Report-Card/Report-Card-2018/ArtMID/7878/ArticleID/778/Arctic-Ocean-Primary-Productivity-The-Response-of-Marine-Algae-to-Climate-Warming-and-Sea-Ice-Decline*.

Frey, K. E., & McClelland, J. W. (2009). Impacts of permafrost degradation on arctic river biogeochemistry. *Hydrological Processes*, *23*(1), 169–182. https://doi.org/10.1002/hyp.7196

Frey, K. E., McClelland, J. W., Holmes, R. M., & Smith, L. C. (2007). Impacts of climate warming and permafrost thaw on the riverine transport of nitrogen and phosphorus to the Kara Sea. *Journal of Geophysical Research: Biogeosciences (2005–2012)*, *112*(G4), n/a-n/a. https://doi.org/10.1029/2006jg000369

Fripiat, F., Sigman, D. M., Fawcett, S. E., Rafter, P. A., Weigand, M. A., & Tison, J. -L. (2014). New insights into sea ice nitrogen biogeochemical dynamics from the nitrogen isotopes. *Global Biogeochemical Cycles*, *28*(2), 115–130. https://doi.org/10.1002/2013gb004729

Granger, J., & Sigman, D. M. (2009). Removal of nitrite with sulfamic acid for nitrate N and O isotope analysis with the denitrifier method. *Rapid Communications in Mass Spectrometry*, *23*(23), 3753–3762. https://doi.org/10.1002/rcm.4307

Granger, J., Sigman, D. M., Needoba, J. A., & Harrison, P. J. (2004). Coupled nitrogen and oxygen isotope fractionation of nitrate during assimilation by cultures of marine phytoplankton. *Limnology and Oceanography*, *49*(5), 1763–1773. https://doi.org/10.4319/lo.2004.49.5.1763

Granger, J., Sigman, D. M., Gagnon, J., Tremblay, J., & Mucci, A. (2018). On the Properties of the Arctic Halocline and Deep Water Masses of the Canada Basin from Nitrate Isotope Ratios. *Journal of Geophysical Research: Oceans*, *123*(8), 5443–5458. https://doi.org/10.1029/2018jc014110

Hastings, M. G., Steig, E. J., & Sigman, D. M. (2004). Seasonal variations in N and O isotopes of nitrate in snow at Summit, Greenland: Implications for the study of nitrate

in snow and ice cores. *Journal of Geophysical Research: Atmospheres (1984–2012)*, *109*(D20). https://doi.org/10.1029/2004jd004991

Heikoop, J. M., Throckmorton, H. M., Newman, B. D., Perkins, G. B., Iversen, C. M., Chowdhury, T. R., et al. (2015). Isotopic identification of soil and permafrost nitrate sources in an Arctic tundra ecosystem. *Journal of Geophysical Research: Biogeosciences*, *120*(6), 1000–1017. https://doi.org/10.1002/2014jg002883

Hill, V. J., Light, B., Steele, M., & Zimmerman, R. C. (2018). Light Availability and Phytoplankton Growth Beneath Arctic Sea Ice: Integrating Observations and Modeling. *Journal of Geophysical Research: Oceans*, *123*(5), 3651–3667. https://doi.org/10.1029/2017jc013617

Holland, A. T., Williamson, C. J., Sgouridis, F., Tedstone, A. J., McCutcheon, J., Cook, J. M., et al. (2019). Dissolved organic nutrients dominate melting surface ice of the Dark Zone (Greenland Ice Sheet). *Biogeosciences*, *16*(16), 3283–3296. https://doi.org/10.5194/bg-16-3283-2019

Holmes, R. M., McClelland, J. W., Peterson, B. J., Tank, S. E., Bulygina, E., Eglinton, T. I., et al. (2012). Seasonal and annual fluxes of nutrients and organic matter from large rivers to the Arctic Ocean and surrounding seas. *Estuaries and Coasts*, *35*(2), 369--382.

Hopkinson, C. S., Fry, B., & Nolin, A. L. (1997). Stoichiometry of dissolved organic matter dynamics on the continental shelf of the northeastern U.S.A. *Continental Shelf Research*, *17*(5), 473–489. https://doi.org/10.1016/s0278-4343(96)00046-5

Johnston, J. C., & Thiemens, M. H. (1997). The isotopic composition of tropospheric ozone in three environments. *Journal of Geophysical Research: Atmospheres*, *102*(D21), 25395–25404. https://doi.org/10.1029/97jd02075

Jones, E. P., Anderson, L. G., & Swift, J. H. (1998). Distribution of Atlantic and Pacific waters in the upper Arctic Ocean: Implications for circulation. *Geophysical Research Letters*, *25*, 765–768.

Kaiser, K., Canedo-Oropeza, M., McMahon, R., & Amon, R. M. W. (2017). Origins and transformations of dissolved organic matter in large Arctic rivers. *Scientific Reports*, *7*(1), 13064. https://doi.org/10.1038/s41598-017-12729-1

Kiddon, J., Bender, M. L., Orchardo, J., Caron, D. A., Goldman, J. C., & Dennett, M. (1993). Isotopic fractionation of oxygen by respiring marine organisms. *Global Biogeochemical Cycles*, *7*(3), 679–694.

Knapp, A. N., Sigman, D. M., & Lipschultz, F. (2005). N isotopic composition of dissolved organic nitrogen and nitrate at the Bermuda Atlantic Time-series Study site. *Global Biogeochemical Cycles*, *19*(1).

Knapp, A. N., Casciotti, K. L., & Prokopenko, M. G. (2018). Dissolved Organic Nitrogen Production and Consumption in Eastern Tropical South Pacific Surface Waters. *Global Biogeochemical Cycles*, *32*(5), 769–783. https://doi.org/10.1029/2017gb005875

Knapp, A N., Sigman, D. M., & Lipschultz, F. (2005). N isotopic composition of dissolved organic nitrogen and nitrate at the Bermuda Atlantic Time-series Study site. *Global Biogeochemical Cycles*, *19*(1). https://doi.org/10.1029/2004gb002320

Krankowsky, D., Bartecki, F., Klees, G. G., Mauersberger, K., Schellenbach, K., & Stehr, J. (1995). Measurement of heavy isotope enrichment in tropospheric ozone. *Geophysical Research Letters*, *22*(13), 1713–1716. https://doi.org/10.1029/95gl01436

Lehmann, N., Kienast, M., Granger, J., Bourbonnais, A., Altabet, M. A., & Tremblay, J. -É. (2019). Remote Western Arctic Nutrients Fuel Remineralization in Deep Baffin Bay. *Global Biogeochemical Cycles*, *33*(6), 649–667. https://doi.org/10.1029/2018gb006134

Letscher, R. T., Hansell, D. A., Kadko, D., & Bates, N. R. (2013). Dissolved organic nitrogen dynamics in the Arctic Ocean. *Marine Chemistry*, *148*, 1–9. https://doi.org/10.1016/j.marchem.2012.10.002

Letscher, R. T., Hansell, D. A., Carlson, C. A., Lumpkin, R., & Knapp, A. N. (2013). Dissolved organic nitrogen in the global surface ocean: Distribution and fate. *Global Biogeochemical Cycles*, *27*(1), 141–153. https://doi.org/10.1029/2012gb004449

Lobbes, J. M., Fitznar, H. P., & Kattner, G. (2000). Biogeochemical characteristics of dissolved and particulate organic matter in Russian rivers entering the Arctic Ocean. *Geochimica et Cosmochimica Acta*, *26*, 2973–2983.

Louiseize, N. L., Lafrenière, M. J., & Hastings, M. G. (2014). Stable isotopic evidence of enhanced export of microbially derived NO3- following active layer slope disturbance in the Canadian High Arctic. *Biogeochemistry*, *121*(3), 565–580. https://doi.org/10.1007/s10533-014-0023-x

Maita, Y., & Yanada, M. (1990). Vertical distribution of total dissolved nitrogen and dissolved organic nitrogen in seawater. *Geochemical Journal*, *24*(4), 245–254.

McClelland, J. W., Holmes, R. M., Peterson, B. J., Raymond, P. A., Striegl, R. G., Zhulidov, A. V., et al. (2016). Particulate organic carbon and nitrogen export from major Arctic rivers. *Global Biogeochemical Cycles*, *30*(5), 629–643. https://doi.org/10.1002/2015gb005351

Minagawa, M., & Wada, E. (1986). Nitrogen isotope ratios of red tide organisms in the East China Sea: A characterization of biological nitrogen fixation. *Marine Chemistry*, *19*(3), 245–259. https://doi.org/10.1016/0304-4203(86)90026-5

Moschonas, G., Gowen, R. J., Paterson, R. F., Mitchell, E., Stewart, B. M., McNeill, S., et al. (2017). Nitrogen dynamics and phytoplankton community structure: the role of organic nutrients. *Biogeochemistry*, *134*(1–2), 125–145. https://doi.org/10.1007/s10533-017-0351-8

Peterson, B. J., Holmes, R. M., McClelland, J. W., Vörösmarty, C. J., Lammers, R. B., Shiklomanov, A. I., et al. (2002). Increasing River Discharge to the Arctic Ocean. *Science*, *298*(5601), 2171–2173. https://doi.org/10.1126/science.1077445

Pfeffer, W. T., Arendt, A. A., Bliss, A., Bolch, T., Cogley, J. G., Gardner, A. S., et al. (2014). The Randolph Glacier Inventory: a globally complete inventory of glaciers. *Journal of Glaciology*, *60*(221), 537–552. https://doi.org/10.3189/2014jog13j176

Rafter, P. A., DiFiore, P. J., & Sigman, D. M. (2013). Coupled nitrate nitrogen and oxygen isotopes and organic matter remineralization in the Southern and Pacific Oceans. *Journal of Geophysical Research: Oceans*, *118*(10), 4781–4794. https://doi.org/10.1002/jgrc.20316

Rood, S. B., Kaluthota, S., Philipsen, L. J., Rood, N. J., & Zanewich, K. P. (2017). Increasing discharge from the Mackenzie River system to the Arctic Ocean. *Hydrological Processes*, *31*(1), 150–160. https://doi.org/10.1002/hyp.10986

Schlitzer, R. (2021). Ocean Data Viewer. Retrieved from https://odv.awi.de

Sherwood, O. A., Davin, S. H., Lehmann, N., Buchwald, C., Edinger, E. N., Lehmann, M. F., & Kienast, M. (2021). Stable isotope ratios in seawater nitrate reflect the influence of Pacific water along the Northwest Atlantic margin. *Biogeosciences Discussions*, *2021*, 1–32. https://doi.org/10.5194/bg-2021-45

Sigman, D. M., & Casciotti, K. L. (2001). Nitrogen Isotopes in the Ocean. In *Encyclopedia of Ocean Sciences* (pp. 1884–1894).

Silsbe, G. M., Behrenfeld, M. J., Halsey, K. H., Milligan, A. J., & Westberry, T. K. (2016). The CAFE model: A net production model for global ocean phytoplankton. *Global Biogeochemical Cycles*, *30*(12), 1756–1777. https://doi.org/10.1002/2016gb005521

Sipler, R., & Bronk, D. (2014). Dynamics of Dissolved Organic Nitrogen. In D. A. Hansel & C. A. Carlson (Eds.), *Biogeochemistry of Dissolved Organic Matter* (Second, pp. 127–232). https://doi.org/10.1016/b978-0-12-405940-5.00004-2

Snyder, L., & Bowden, W. B. (2014). Nutrient dynamics in an oligotrophic arctic stream monitored in situ by wet chemistry methods. *Water Resources Research*, *50*(3), 2039–2049. https://doi.org/10.1002/2013wr014317

Tang, C. C. L., Ross, C. K., Yao, T., Petrie, B., DeTracey, B. M., & Dunlap, E. (2004). The circulation, water masses and sea-ice of Baffin Bay. *Progress in Oceanography*, *63*(4), 183–228. https://doi.org/10.1016/j.pocean.2004.09.005

Tank, S. E., Manizza, M., Holmes, R. M., McClelland, J. W., & Peterson, B. J. (2012). The Processing and Impact of Dissolved Riverine Nitrogen in the Arctic Ocean. *Estuaries and Coasts*, *35*(2), 401–415. https://doi.org/10.1007/s12237-011-9417-3

Telling, J., Stibal, M., Anesio, A. M., Tranter, M., Nias, I., Cook, J., et al. (2012). Microbial nitrogen cycling on the Greenland Ice Sheet. *Biogeosciences*, *9*(7), 2431–2442. https://doi.org/10.5194/bg-9-2431-2012

Thibodeau, B., Bauch, D., & Voss, M. (2017). Nitrogen dynamic in Eurasian coastal Arctic ecosystem: Insight from nitrogen isotope. *Global Biogeochemical Cycles*, *31*(5), 836–849. https://doi.org/10.1002/2016gb005593

Torres-Valdés, S., Roussenov, V. M., Sanders, R., Reynolds, S., Pan, X., Mather, R., et al. (2009). Distribution of dissolved organic nutrients and their effect on export production over the Atlantic Ocean. *Global Biogeochemical Cycles*, *23*(4), n/a-n/a. https://doi.org/10.1029/2008gb003389

Tremblay, J., Gratton, Y., Carmack, E. C., Payne, C. D., & Price, N. M. (2002). Impact of the large-scale Arctic circulation and the North Water Polynya on nutrient inventories in Baffin Bay. *Journal of Geophysical Research: Oceans (1978–2012)*, *107*(C8), 26-1-26–14. https://doi.org/10.1029/2000jc000595

Tremblay, J.-É., Raimbault, P., Garcia, N., Lansard, B., Babin, M., & Gagnon, J. (2014). Impact of river discharge, upwelling and vertical mixing on the nutrient loading and productivity of the Canadian Beaufort Shelf. *Biogeosciences*, *11*(17), 4853–4868. https://doi.org/10.5194/bg-11-4853-2014

Tremblay, Jean-Éric, Michel, C., Hobson, K. A., Gosselin, M., & Price, N. M. (2006). Bloom dynamics in early opening waters of the Arctic Ocean. *Limnology and Oceanography*, *51*(2), 900–912. https://doi.org/10.4319/lo.2006.51.2.0900

Tremblay, Jean-Éric, Anderson, L. G., Matrai, P., Coupel, P., Bélanger, S., Michel, C., & Reigstad, M. (2015). Global and regional drivers of nutrient supply, primary production and CO2 drawdown in the changing Arctic Ocean. *Progress in Oceanography*, *139*, 171–196. https://doi.org/10.1016/j.pocean.2015.08.009

Vonk, J. E., Tank, S. E., Bowden, W. B., Laurion, I., Vincent, W. F., Alekseychik, P., et al. (2015). Reviews and syntheses: Effects of permafrost thaw on Arctic aquatic ecosystems. *Biogeosciences*, *12*(23), 7129–7167. https://doi.org/10.5194/bg-12-7129-2015

Wadham, J. L., Hawkings, J., Telling, J., Chandler, D., Alcock, J., O'Donnell, E., et al. (2016). Sources, cycling and export of nitrogen on the Greenland Ice Sheet. *Biogeosciences*, *13*(22), 6339–6352. https://doi.org/10.5194/bg-13-6339-2016

Wagner, D., Spieck, E., Bock, E., & Pfeiffer, E.-M. (2002). Microbial Life in Terrestrial Permafrost: Methanogenesis and Nitrification in Gelisols as Potentials for Exobiological Process (p. 143). Berlin, Heidelberg: Springer Berlin Heidelberg. https://doi.org/10.1007/978-3-642-59381-9_10

Wang, X., & Veizer, J. (2000). Respiration–photosynthesis balance of terrestrial aquatic ecosystems, Ottawa area, Canada. *Geochimica et Cosmochimica Acta*, *64*(22), 3775–3786. https://doi.org/10.1016/s0016-7037(00)00477-4

Wassmann, P., Duarte, C. M., Agusti, S., & Sejr, M. K. (2011). Footprints of climate change in the Arctic marine ecosystem. *Global Change Biology*, *17*(2), 1235–1249. https://doi.org/10.1111/j.1365-2486.2010.02311.x

Wu, P., Wood, R., & Stott, P. (2005). Human influence on increasing Arctic river discharges. *Geophysical Research Letters*, *32*(2). https://doi.org/10.1029/2004gl021570

Wynn, P. M., Hodson, A. J., Heaton, T. H. E., & Chenery, S. R. (2007). Nitrate production beneath a High Arctic glacier, Svalbard. *Chemical Geology*, *244*(1–2), 88–102. https://doi.org/10.1016/j.chemgeo.2007.06.008

Yamamoto-Kawai, M., Carmack, E., & McLaughlin, F. (2006). Nitrogen balance and Arctic throughflow. *Nature*, *443*(7107), 43–43. https://doi.org/10.1038/443043a

Yamamoto-Kawai, M., McLaughlin, F. A., Carmack, E. C., Nishino, S., & Shimada, K. (2008). Freshwater budget of the Canada Basin, Arctic Ocean, from salinity, δ18O, and nutrients. *Journal of Geophysical Research: Oceans (1978–2012)*, *113*(C1). https://doi.org/10.1029/2006jc003858

Ye, F., Guo, W., Wei, G., & Jia, G. (2018). The Sources and Transformations of Dissolved Organic Matter in the Pearl River Estuary, China, as Revealed by Stable Isotopes. *Journal of Geophysical Research: Oceans*, *123*(9), 6893–6908. https://doi.org/10.1029/2018jc014004

APPENDIX A

RIVER ISOTOPIC MODEL DETAILS

Model for NO_3^- in Arctic glacial rivers

a = nitrified NO_3^- (from permafrost or atmospheric NH_4^+)

b = atmospheric NO_3^- (from glacial snow melt)

d = assimilation of NO_3^-

e = recycled production of NO_3^-

$\delta^{15}N_{nit}$= $\delta^{15}N$ of NO_3^- produced though nitrification of ammonium, 1.22 (-6-10‰; Arendt et al. 2016; Heikoop et al. 2016)

$\delta^{18}O_{nit}$= $\delta^{18}O$ of NO_3^- produced though nitrification of ammonium, -14.21‰ (-19.51—8.9; assuming $\delta^{18}O$ DO of 23.5-24.2‰ (Kiddon et al., 1993; Wang & Veizer, 2000; Horibe et al., 1973 as in Wynn et al., 2007) and $\delta^{18}O$ H_2O of -12--22‰ (Arendt et al. 2016, Wynn et al., 2007))

$\delta^{15}N_{atm}$ = $\delta^{15}N$ of NO_3^- from atmospheric deposition, -3.54‰ (-8.72-1.40; Ansari et al., 2013; Hastings et al., 2003; Heikoop et al., 2015; Louiseize et al., 2014)

$\delta^{18}O_{atm}$ = $\delta^{18}O$ of NO_3^- from atmospheric deposition, 72.07‰ (60.30-80.20; Ansari et al., 2013; Hastings et al., 2003; Heikoop et al., 2015; Louiseize et al., 2014)

ε_{as}^{15} = isotope effect of NO_3^- assimilation on N

ε_{as}^{18} = isotope effect of NO_3^- assimilation on O

$\delta^{15}N_{re}$ = $\delta^{15}N$ of NO_3^- from recycled production

$\delta^{18}O_{re}$ = $\delta^{18}O$ of NO_3^- from recycled production -14.21‰ (-19.51--8.9; assuming $\delta^{18}O$ DO of 23.5-24.2‰ (Kiddon et al., 1993; Wang & Veizer, 2000; Horibe et al., 1973 as in Wynn et al., 2007) and $\delta^{18}O$ H_2O of -12--22‰ (Arendt et al. 2016, Wynn et al., 2007))

$\delta^{15}N_{as}$ = $\delta^{15}N_{box}$ - ε_{as}^{15} = $\delta^{15}N$ of NO_3^- assimilated

$\delta^{15}N_{box}$ = model output of $\delta^{15}N$ of NO_3^- in the river

Scenario 1

- Nitrified NO_3^- is a source

- Atmospheric NO_3^- is a source
- NO_3^- assimilation is a sink
- Recycled production accounts for 45% of supplied NO_3^-
- No denitrification

For $\delta^{15}N$

$$\delta^{15}N_{box} = a \times \delta^{15}N_{nit} + b \times \delta^{15}N_{atm} - [(d - e) \times (\delta^{15}N_{box} - \varepsilon_{as}^{15})]$$

This can be arranged to

$$\delta^{15}N_{box} = \frac{a \times \delta^{15}N_{nit} + b \times \delta^{15}N_{atm} + [(d - e) \times \varepsilon_{as}^{15}]}{(1 + d - e)}$$

For $\delta^{18}O$

$$\delta^{18}O_{box} = a \times \delta^{18}O_{nit} + b \times \delta^{18}O_{atm} - [d \times (\delta^{18}O_{box} - \varepsilon_{as}^{18})] + e \times \delta^{18}O_{re}$$

This can be arranged to

$$\delta^{18}O_{box} = \frac{a \times \delta^{18}O_{nit} + b \times \delta^{18}O_{atm} + d \times \varepsilon_{as}^{18} + e \times \delta^{18}O_{re}}{(1 + d)}$$

Scenario 2

- Nitrified NO_3^- is a source
- Atmospheric NO_3^- is a source
- NO_3^- assimilation is a sink
- Recycled production accounts for 30% of supplied NO_3^-
- No denitrification

This uses the same equation as Scenario 2, but with a different fraction of recycled production (e).

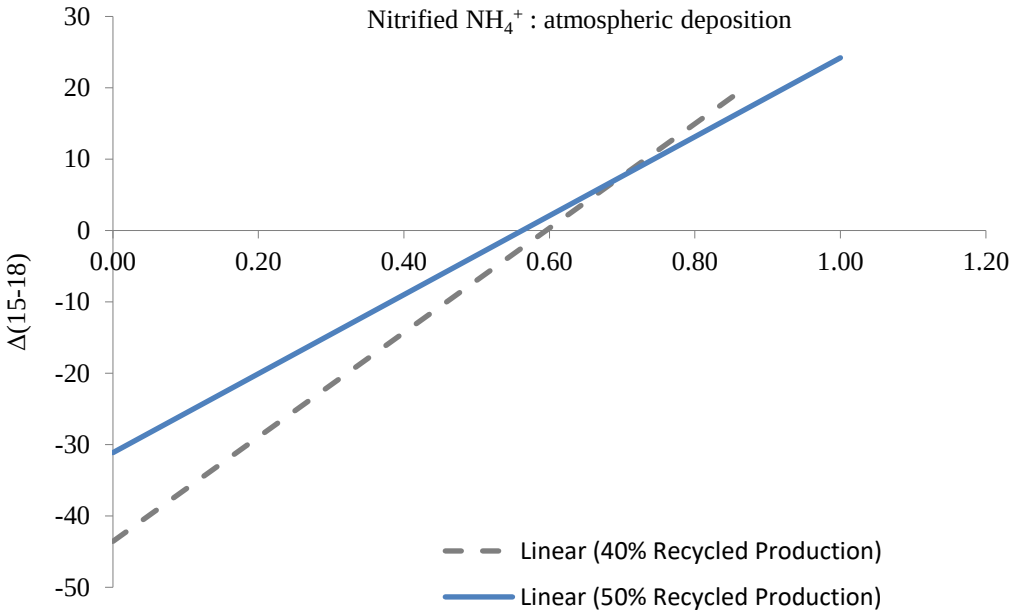

Figure A.1: Isotopic model for NO_3^- cycling, the ratio of nitrified NH_4^+: atmospheric deposition is on the x axis, and Δ(15-18) on the y-axis. The solid blue line represents Scenario 1, and the dashed grey line represents Scenario 2.

APPENDIX B

SUPPLEMENTARY FIGURES

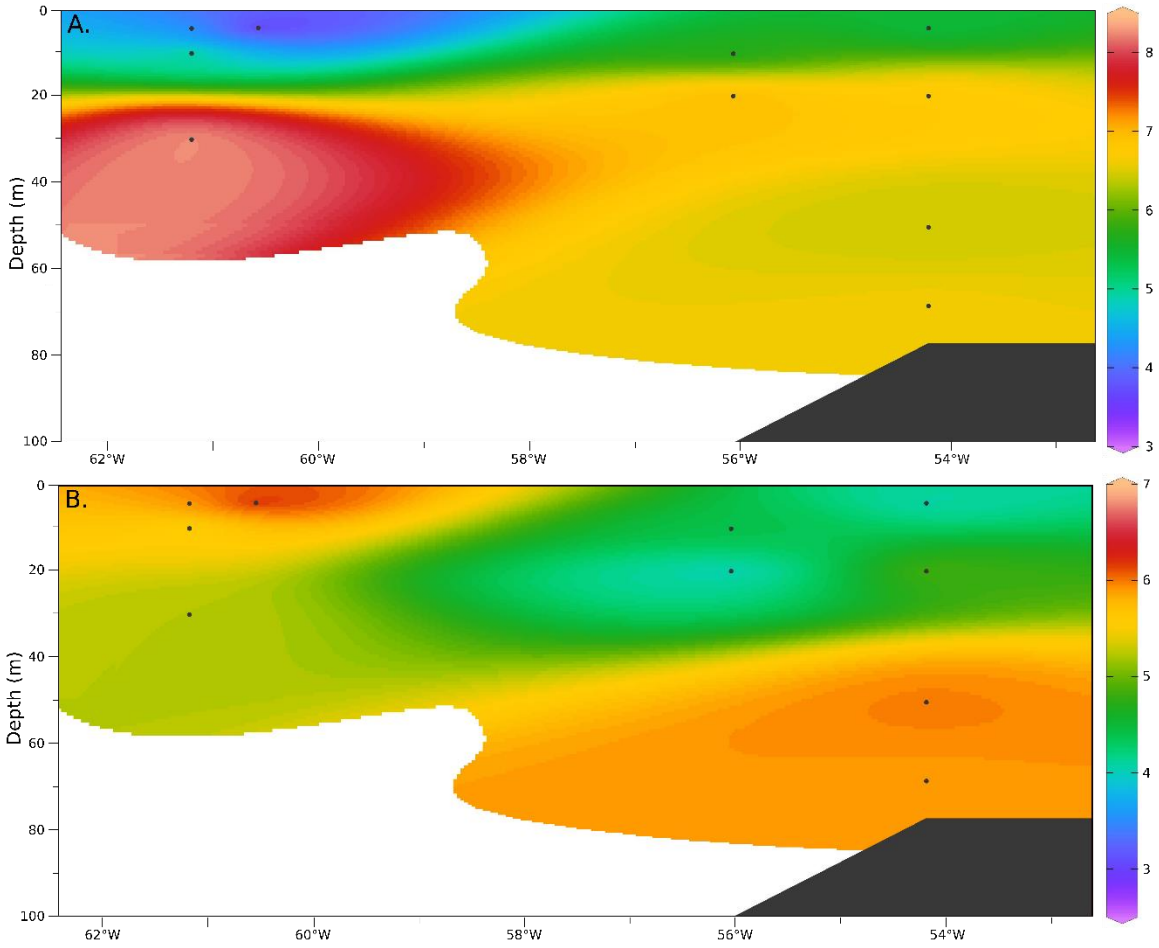

Figure B.1: A. [DON] and B. $\delta^{15}N$ of DON at depth in Transect 1

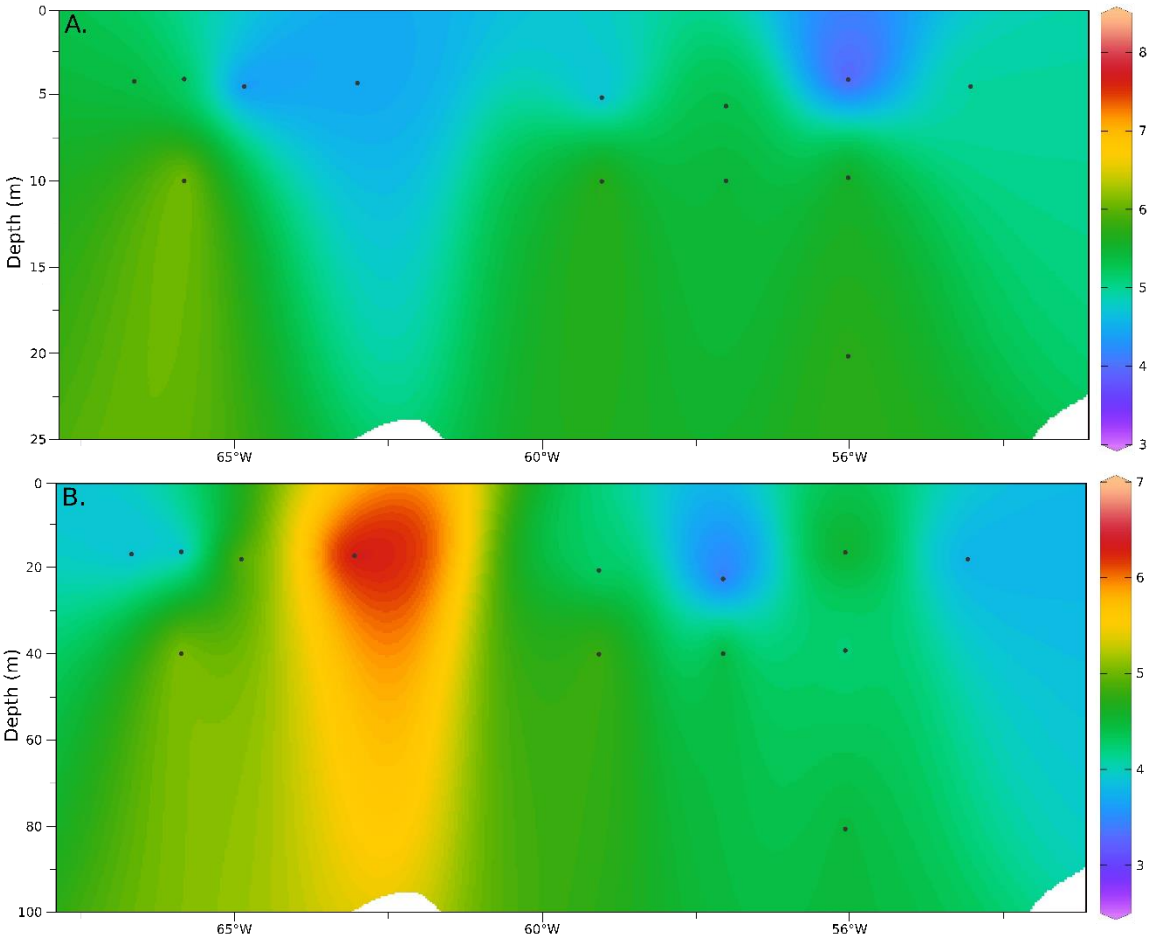

Figure B.2: A. [DON] and B. $\delta^{15}N$ of DON at depth in Transect 2

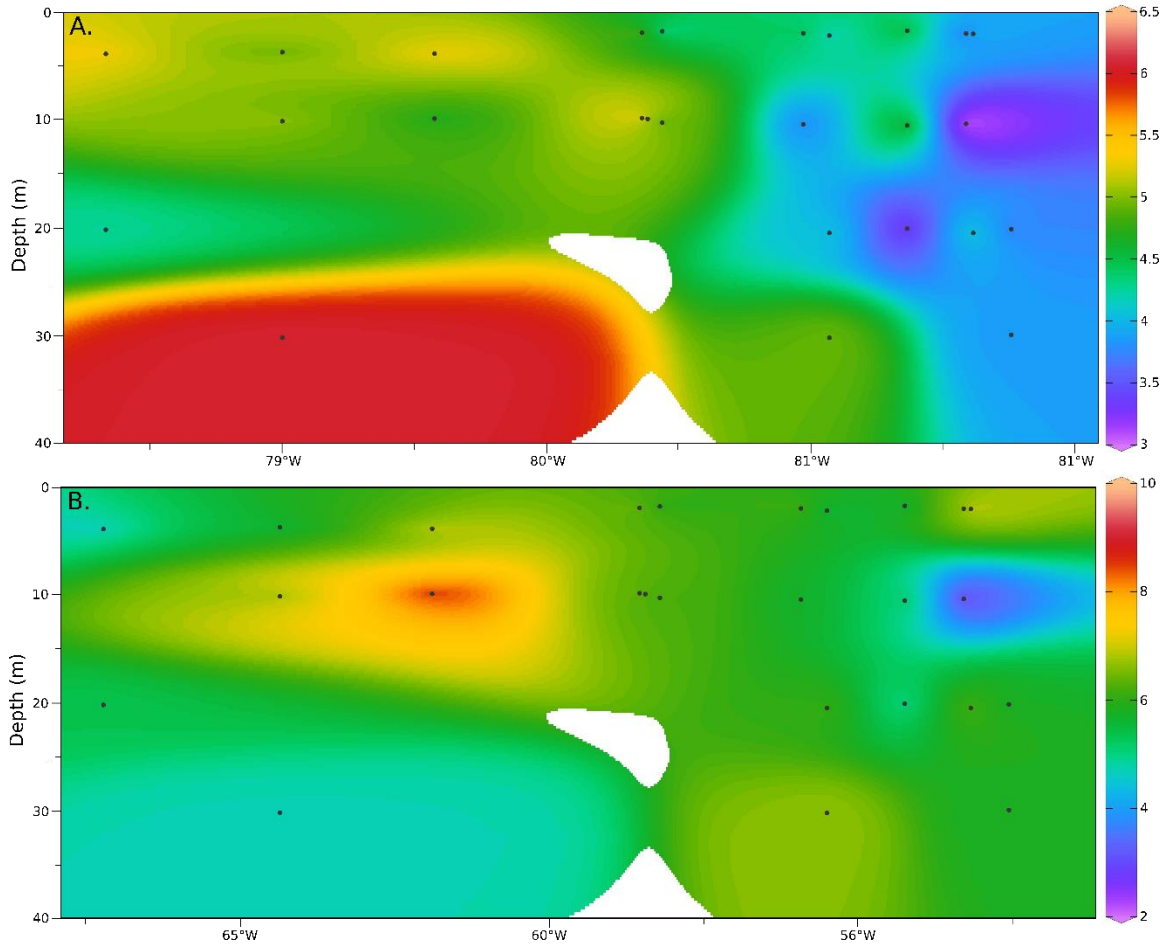

Figure B.3: A. [DON] and B. $\delta^{15}N$ of DON at depth in Nares Strait

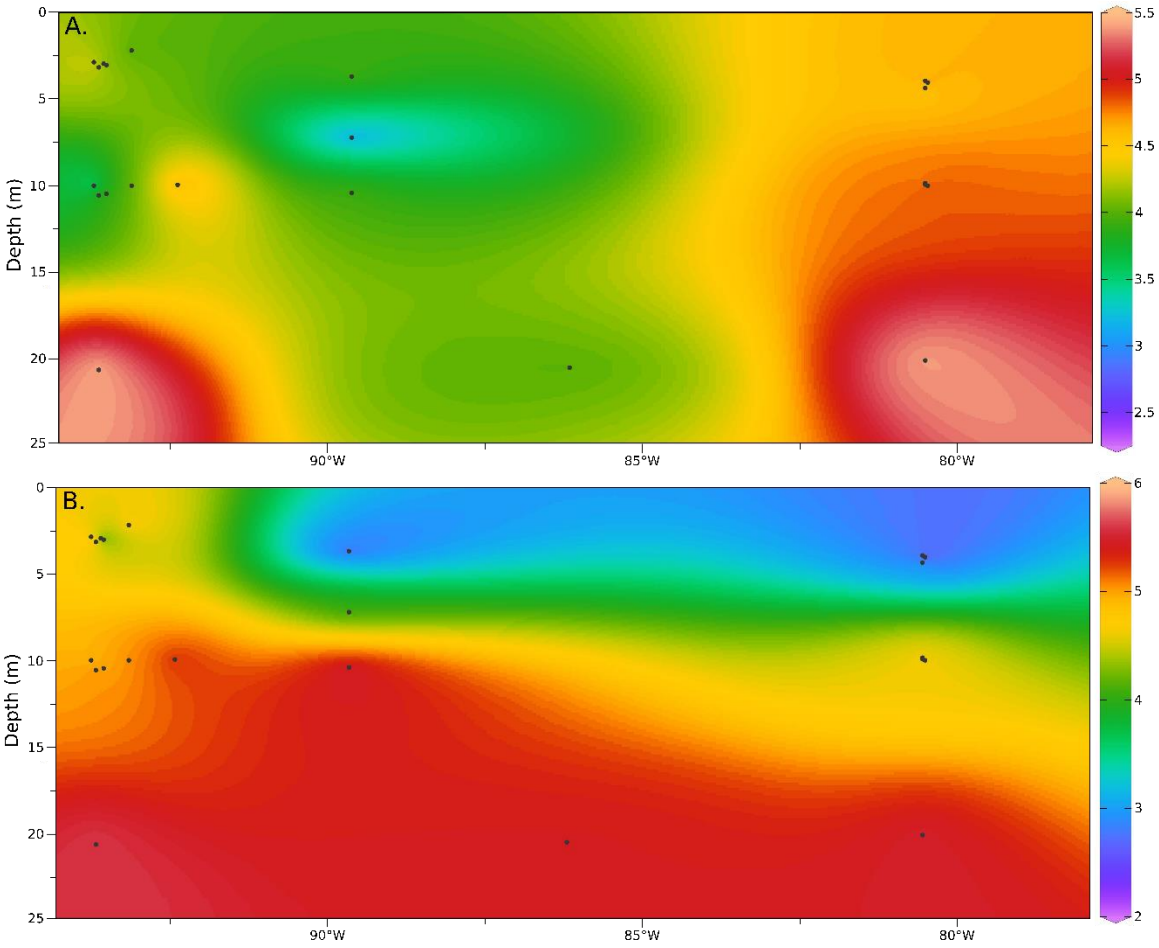

Figure B.4: A. [DON] and B. $\delta^{15}N$ of DON at depth in Lancaster Sound

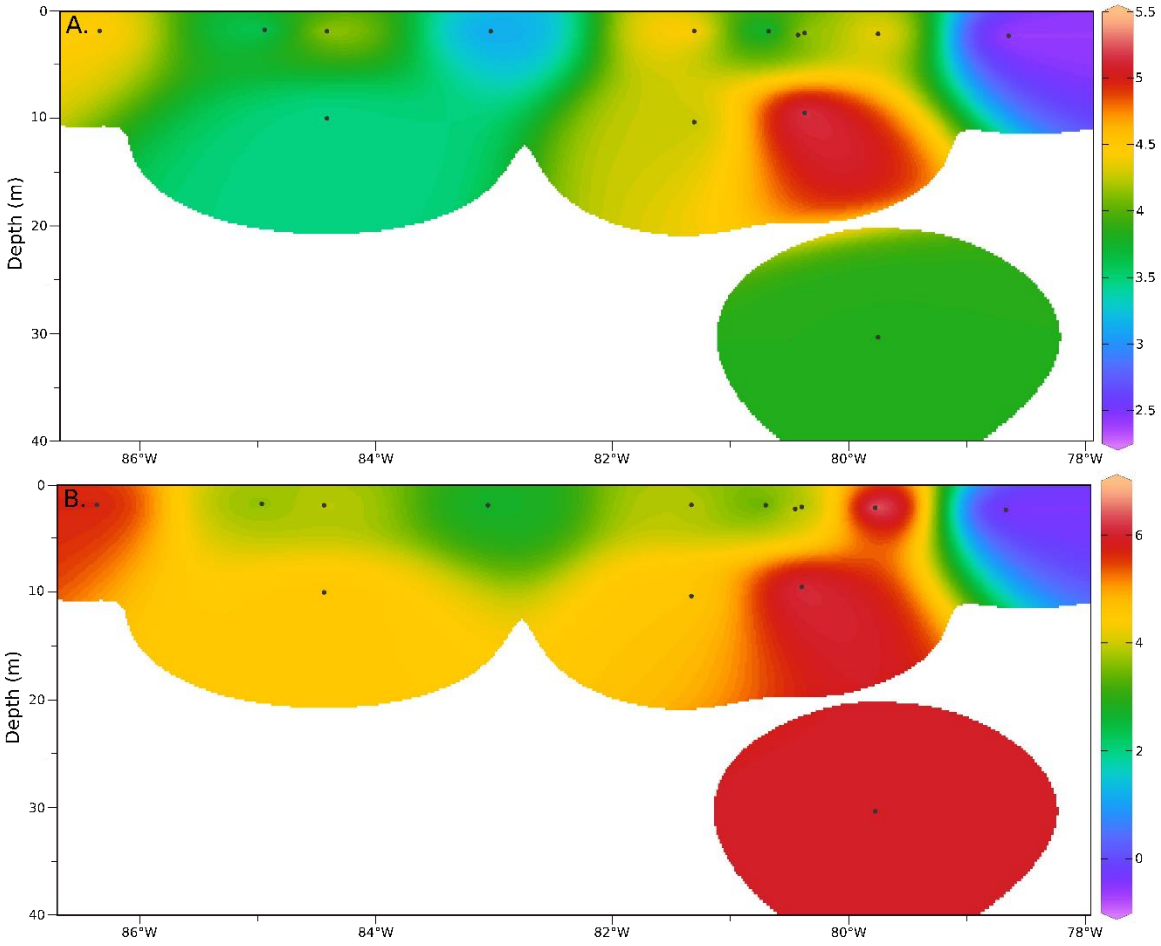

Figure B.5: A. [DON] and B. $\delta^{15}N$ of DON at depth in Jones Sound

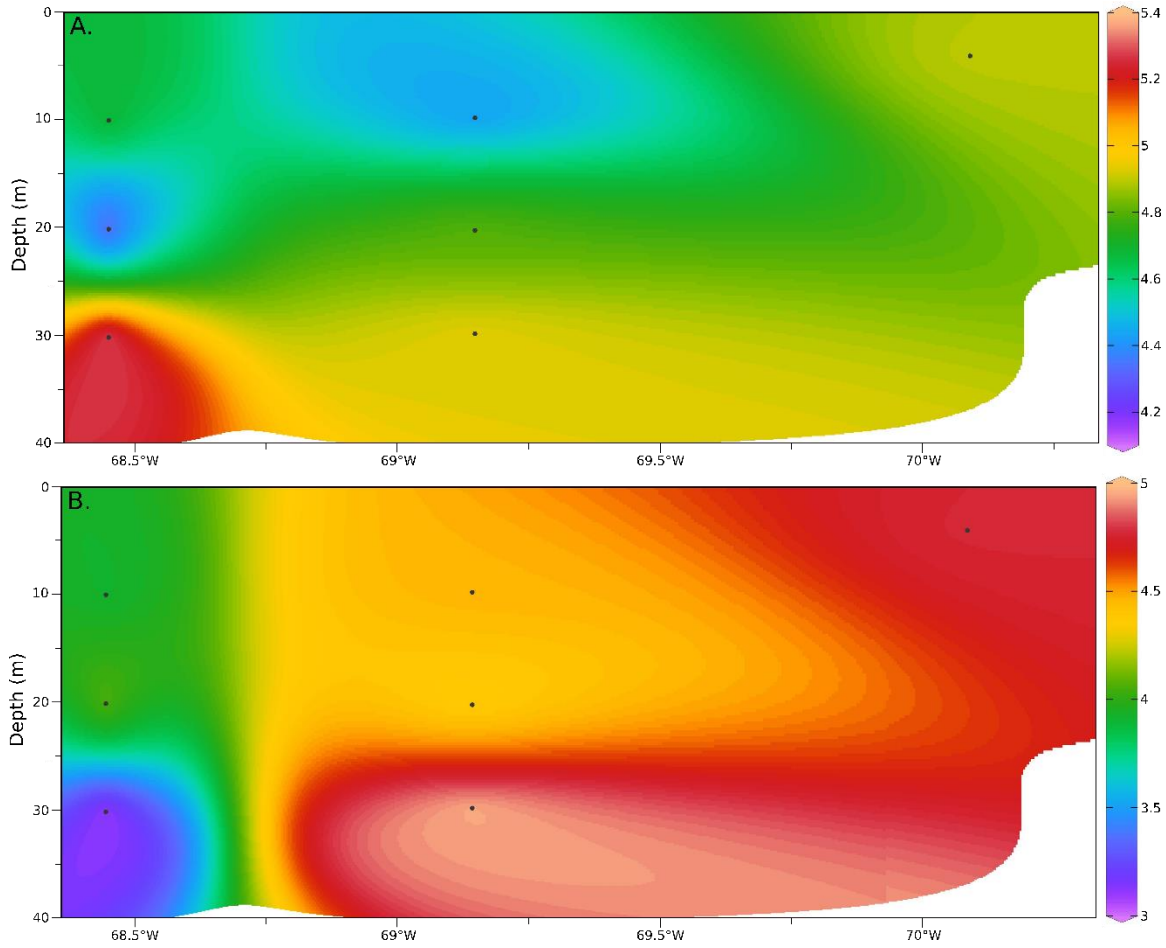

Figure B.6: A. [DON] and B. $\delta^{15}N$ of DON at depth near Disko Island

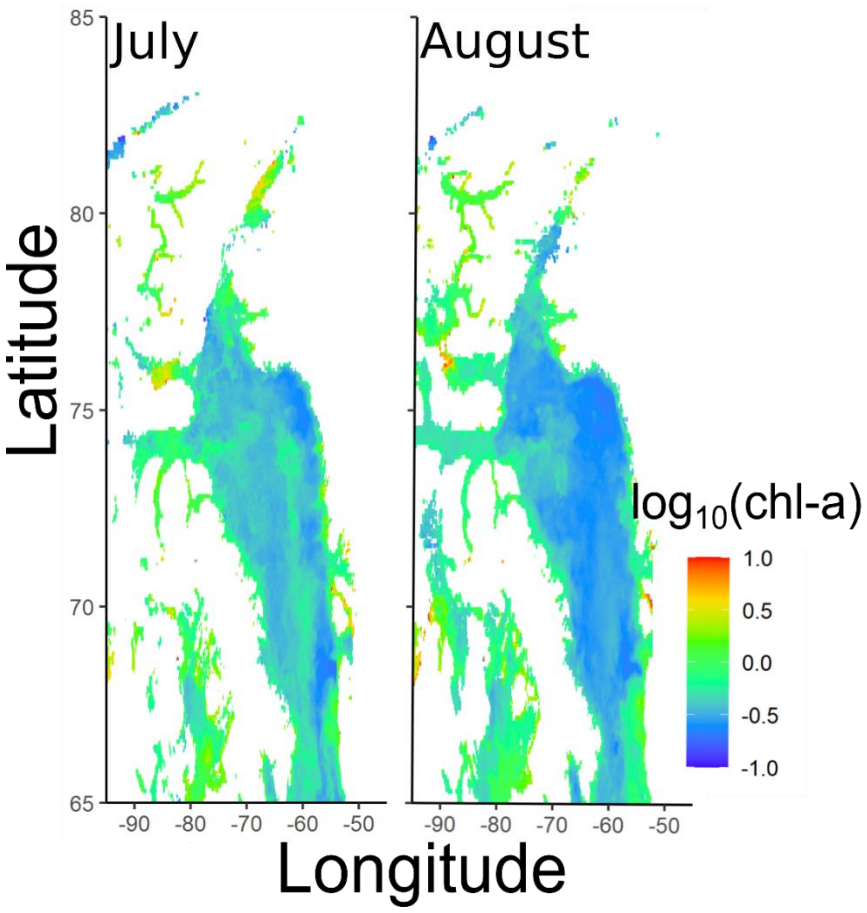

Figure B.7: Average surface chlorophyll-a derived from MODIS-AQUA data for July and August 2019

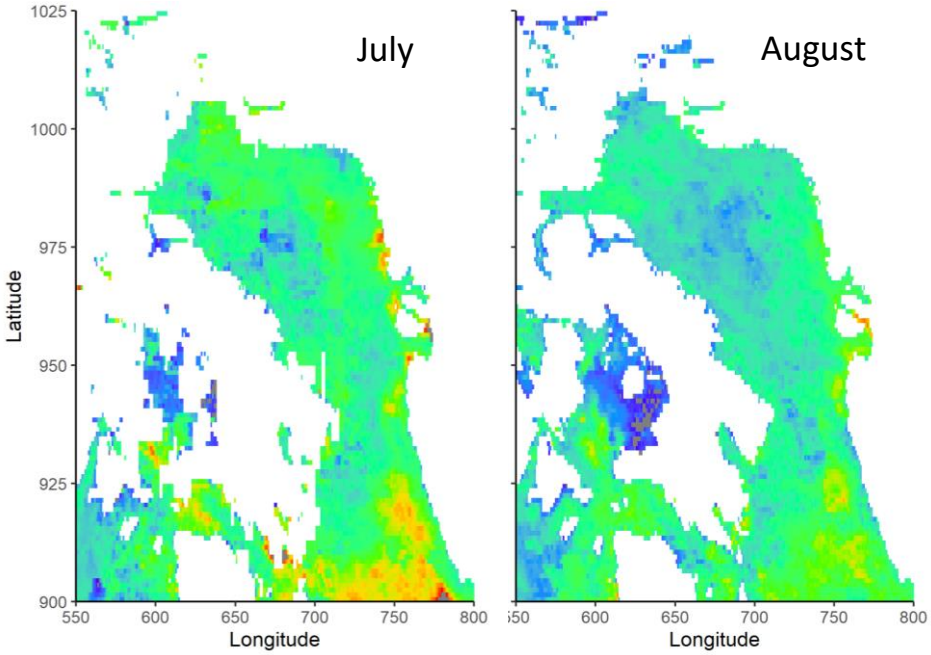

Figure B.8: Primary productivity in Baffin Bain for July and August 2019 from the CAFE model (Silsbe et al., 2016)

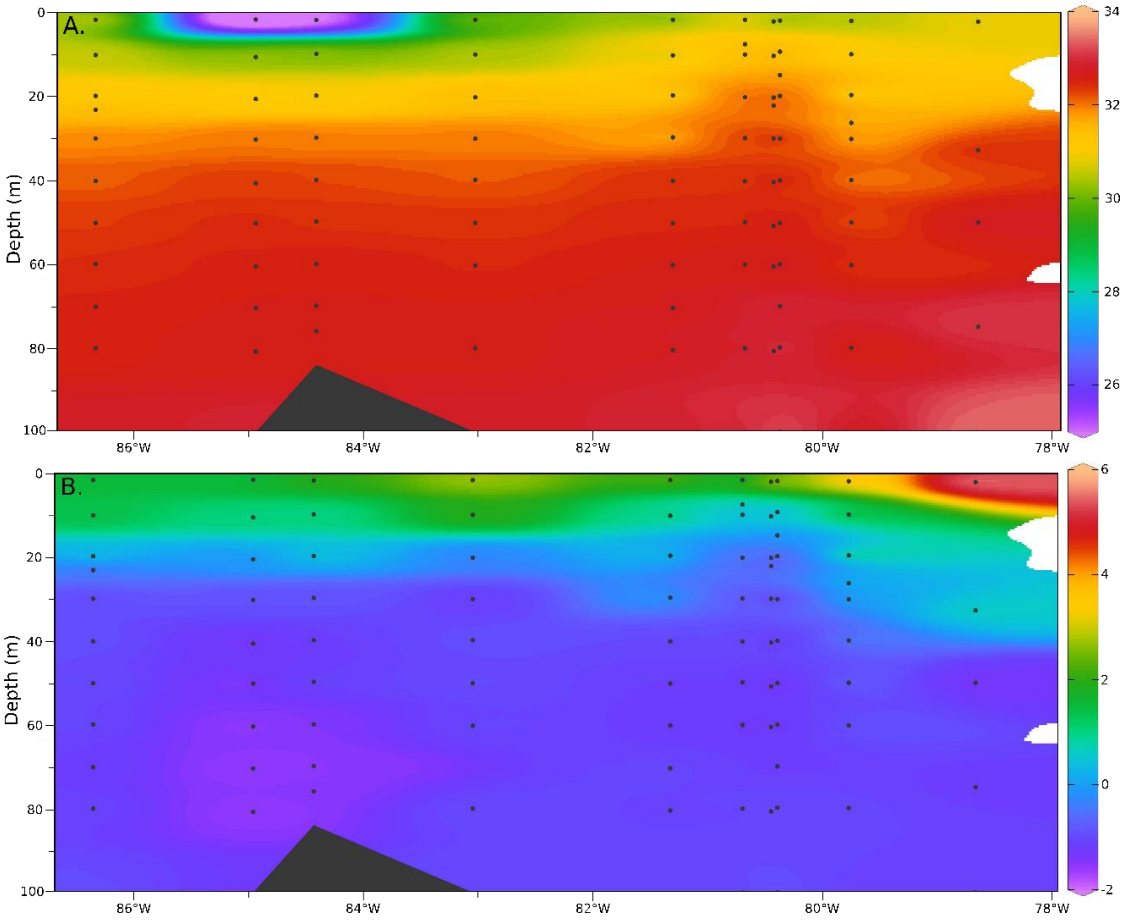

Figure B.9: A. Temperature and B. Salinity cross sections in Jones Sound

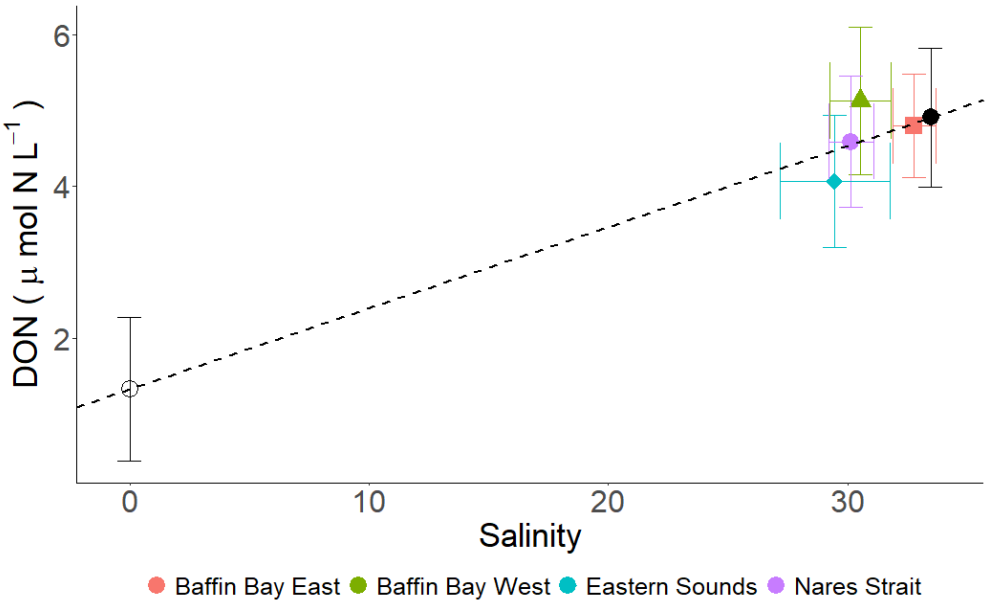

Figure B.10: Average [DON] (µM N L^{-1}) in the upper 10 meters of the water column vs average salinity for the following regions: eastern Baffin Bay (pink square), western Baffin Bay (green triangle), eastern Sounds (Jones & Lancaster Sounds; blue diamond), and Nares Strait (purple circle) Riverine (hollow) and marine (solid) end members are marked with black dots with solid lines representing standard deviation in our estimates. The dashed line represents mixing between the two end members.

APPENDIX C

RAW DATA

Table C.1: Concentrations of NO_2^-, NO_3^-, DIN, in µM and $\delta^{15}N$ and $\delta^{18}O$ (‰) in ECAA; *denotes data analyzed by Tremblay's lab (Laval University) but not presented here.

Station	*Depth*	*Longitude*	*Latitude*	*NO_2^-*	*NO_3^-*	*DIN*	*$\delta^{15}N\ NO_3$*	*±sd*	*$\delta^{18}O\ NO_3^-$*	*±sd*
units	*m*	°E	°W	µM	µM	µM	‰	‰	‰	‰
115	4.12	288.80	76.33	0.00	0.70	0.70				
132	30.08	287.68	79.00	0.00	1.50	1.50	12.49	0.10	3.63	0.76
136	19.36	292.31	80.36	0.00	5.41	5.41				
135	19.89	291.07	80.44	0.00	2.35	2.35	9.82	0.02	-14.21	0.42
135	29.99	291.07	80.44	0.00	1.64	1.64	9.44	0.15	-10.75	0.68
138	10.35	294.64	81.59	0.00	0.89	0.89	14.84	0.50		
Talbot	7.61	282.95	77.84	0.00	1.87	1.87	11.17	0.22	-9.29	0.53
117	20.12	282.96	77.33	0.00	0.69	0.69	18.00	0.43	6.74	0.32
117	30.38	282.96	77.33	0.00	3.11	3.11	10.91	0.07	-9.83	0.49
290	2.15	282.50	76.36	0.00	0.00	0.00				
290	10.54	282.50	76.36	0.00	0.86	0.86				
292	2.27	279.58	75.85	0.00	0.18	0.18				
292	10.49	279.58	75.85	0.00	0.61	0.61	10.68	0.85	21.80	1.15
292	20.42	279.58	75.85	0.00	4.05	4.05				

292	40.51	279.58	75.85	0.00	7.60	7.60				
293	500.60	279.33	75.73	0.00	14.44	14.44				
site 2.3	1.91	276.98	76.13	0.00	1.05	1.05	15.01	1.29	11.61	2.20
site 2.3	10.13	276.98	76.13	0.00	0.62	0.62				
site 2.3	30.16	276.98	76.13	0.00	4.61	4.61				
site 2.3	39.96	276.98	76.13	0.00	9.72	9.72				
Site 1.4	1.79	275.06	76.50	0.00	1.32	1.32	10.65	1.13	28.79	2.78
Site 1.4	40.77	275.06	76.50	0.00	4.47	4.47				
297	1.90	278.70	76.37	0.00	0.99	0.99	13.50	1.00	6.61	0.64
297	10.33	278.70	76.37	0.00	1.02	1.02	11.81	0.16	-2.51	2.04
297	19.86	278.70	76.37	0.00	2.08	2.08				
297	29.84	278.70	76.37	0.00	3.27	3.27				
site 2.7	2.35	281.36	75.48	0.00	1.64	1.64				
site 2.7	32.86	281.36	75.48	0.00	0.88	0.88				
305A	10.50	266.48	74.22	0.00	0.92	0.92	15.24	1.24	44.73	0.22
305A	40.69	266.48	74.22	0.00	6.46	6.46				
Wel01	49.93	267.61	74.95	0.00	1.07	1.07				
115	10.14	288.80	76.33			0.23				
111	49.80	286.79	76.31			1.50				
108	9.97	285.40	76.26			0.58	22.38	0.96	60.36	0.50
108	30.03	285.40	76.26			0.25				
126	3.95	286.60	77.35			0.18				
126	10.17	286.60	77.35			0.00				
126	20.50	286.60	77.35			0.00				
126	29.76	286.60	77.35			0.00				
126	40.18	286.60	77.35			1.02				
126	49.96	286.60	77.35			1.46				

132	3.74	287.68	79.00	0.00				
132	10.11	287.68	79.00	0.00				
132	20.11	287.68	79.00	0.00				
132	40.17	287.68	79.00	0.00				
133	3.87	289.71	79.58	0.10				
133	9.88	289.71	79.58	0.00				
133	19.96	289.71	79.58	0.00				
133	30.52	289.71	79.58	0.19				
136	1.96	292.31	80.36	0.63				
136	9.83	292.31	80.36	4.15	9.89	0.12	-14.17	0.23
136	30.02	292.31	80.36	6.99				
136	40.03	292.31	80.36	10.58				
135	1.82	291.07	80.44	0.00				
135	10.23	291.07	80.44	0.00				
135	40.10	291.07	80.44	6.00				
137	7.04	293.99	81.07	0.00				
138	2.02	294.64	81.59	0.39				
117	1.79	282.96	77.33	0.00				
117	10.51	282.96	77.33	0.00				
117	40.09	282.96	77.33	3.67				
117	49.92	282.96	77.33	6.49				
290	20.82	282.50	76.36	0.00				
290	30.67	282.50	76.36	2.46				
290	40.38	282.50	76.36	4.03				
290	50.57	282.50	76.36	5.07				
292	30.08	279.58	75.85	6.41				
site 2.3	20.35	276.98	76.13	1.95				
Site 1.4	10.77	275.06	76.50	0.24				

Site 1.4	20.71	275.06	76.50	0.38
295	1.92	275.59	76.38	1.08
295	9.98	275.59	76.38	0.09
295	19.92	275.59	76.38	0.21
295	29.91	275.59	76.38	0.91
295	39.98	275.59	76.38	4.60
295	49.84	275.59	76.38	7.49
297	40.21	278.70	76.37	8.42
302	7.17	273.84	74.23	0.20
303	7.27	270.38	74.37	0.08
305A	3.07	266.48	74.22	0.08
305A	20.32	266.48	74.22	0.06
305A	30.51	266.48	74.22	3.09
305B	3.00	266.44	74.36	0.00
305B	19.74	266.44	74.36	0.28
Wel01	2.12	267.61	74.95	0.00
Wel01	9.99	267.61	74.95	0.02
Wel01	19.99	267.61	74.95	0.00
Wel01	30.01	267.61	74.95	0.19
Wel02 327	2.25	266.89	75.01	0.02
Wel02 327	10.04	266.89	75.01	0.29
Wel02 327	20.14	266.89	75.01	0.34
Wel02 327	30.11	266.89	75.01	0.20
Wel02 327	50.08	266.89	75.01	1.89
305 D	2.92	266.28	74.60	0.12
305 D	10.03	266.28	74.60	0.29
305 D	20.46	266.28	74.60	1.90
305 D	25.13	266.28	74.60	2.42

305 D	39.96	266.28	74.60			2.61				
190	4.34	298.80	66.59	*	*	*	9.98	0.95	3.35	0.01
190	10.10	298.80	66.59	*	*	*	10.10	0.33	3.24	0.78
190	19.81	298.80	66.59	*	*	*	7.66	0.10	-11.16	0.13
190	29.99	298.80	66.59	*	*	*	9.66	0.01	-5.25	0.21
191	10.44	299.43	66.64	*	*	*	11.25	0.14	-6.10	0.06
193	20.17	300.66	66.77	*	*	*	4.32	0.82	-6.28	0.57
196	19.93	303.94	66.99	*	*	*	6.74	0.01	-0.30	0.02
198	4.24	305.79	67.08	*	*	*	6.50	0.24	3.30	0.02
198	9.95	305.79	67.08	*	*	*	6.26	0.60	6.68	0.35
198	19.93	305.79	67.08	*	*	*	6.86	0.02	3.66	0.17
198	30.01	305.79	67.08	*	*	*	8.59	0.50	-0.60	0.90
198	68.36	305.79	67.08	*	*	*	3.46	0.20	-7.64	0.63
BB18	10.17	307.26	70.09	*	*	*	15.48	0.23	1.22	0.08
226	20.17	300.99	70.70	*	*	*	11.10	0.07	-2.42	0.52
225	10.33	299.00	70.60	*	*	*	11.41	0.14	-1.83	0.23
224	10.17	297.02	70.44	*	*	*	12.00	0.14	0.38	0.11
115	30.25	288.80	76.33	*	*	*	14.56	0.14	3.31	0.34
111	30.00	286.79	76.31	*	*	*	15.57	0.13	1.75	0.87
323	20.26	279.53	74.16	*	*	*	8.81	0.06	-3.35	0.34
325	26.57	279.49	73.82	*	*	*	11.33	0.43	-5.18	0.79
122/site2.8	50.33	284.97	77.34	*	*	*	6.25	0.59		
122/site2.8	100.26	284.97	77.34	*	*	*	4.14	0.12		
134	9.91	291.55	80.39	*	*	*	8.07	0.73	-18.52	2.33
134	20.21	291.55	80.39	*	*	*	7.59	0.06		
134	30.22	291.55	80.39	*	*	*	6.25	0.07		
134	50.19	291.55	80.39	*	*	*	5.61	0.06		
137	30.11	293.99	81.07	*	*	*	11.42	0.02	2.50	0.06

137	40.12	293.99	81.07	*	*	*	9.44	0.10	0.04	0.04
137	49.98	293.99	81.07	*	*	*	8.45	0.02	-1.40	0.14
ken 1	30.04	295.81	81.37	*	*	*	9.14	0.21	-0.56	0.69
ken 1	50.02	295.81	81.37	*	*	*	6.21	0.15		
Rob1	20.08	297.64	81.76	*	*	*	3.90	1.37		
Rob1	29.84	297.64	81.76	*	*	*	9.20	1.22	2.40	0.62
Rob1	50.07	297.64	81.76	*	*	*	5.28	0.50		
6.4	20.42	296.73	81.62	*	*	*	3.42	0.01		
6.4	30.23	296.73	81.62	*	*	*	10.11	0.19		
251b	20.41	298.66	80.97	*	*	*	9.16	0.33	3.18	0.53
251b	30.26	298.66	80.97	*	*	*	6.37	0.38		
251b	50.49	298.66	80.97	*	*	*	4.56	1.56		
Talbot	50.64	282.95	77.84	*	*	*	8.44	1.29	0.96	0.04
291	30.15	279.63	75.99	*	*	*	8.56	0.12		
291	50.19	279.63	75.99	*	*	*	7.37	0.04		
293	10.12	279.33	75.73	*	*	*	9.35	0.05	2.87	0.20
293	20.29	279.33	75.73	*	*	*	6.90	0.78		
293	30.04	279.33	75.73	*	*	*	6.83	0.17		
293	50.02	279.33	75.73	*	*	*	6.05	0.21		
site 2.4	30.11	273.67	76.13	*	*	*	7.20	0.06		
site 2.4	50.19	273.67	76.13	*	*	*	6.54	0.24		
296	30.22	280.25	75.52	*	*	*	11.40	0.31	4.63	0.35
296	50.10	280.25	75.52	*	*	*	8.94	0.05	0.74	0.14
302	20.53	273.84	74.23	*	*	*	12.47	0.54	2.97	0.73
302	30.26	273.84	74.23	*	*	*	12.45	0.07	4.45	0.31
305c	20.66	266.36	74.48	*	*	*	12.43	0.22	0.05	0.71
305c	30.73	266.36	74.48	*	*	*	8.92	1.49	6.62	0.63

Table C.2: Concentration of TDN (µmol N L-1) and $\delta^{15}N$ of TDN (‰) in ECAA.

Station units	*Depth m*	*Longitude °E*	*Latitude °W*	*TDN µmol N L^{-1}*	*±sd µmol N L^{-1}*	*$\delta^{15}N$ TDN ‰*	*±sd ‰*
115	4.12	288.80	76.33	4.92	0.56	3.49	0.65
132	30.08	287.68	79.00	7.59	0.46	6.27	0.22
135	19.89	291.07	80.44	7.28	0.14	6.40	0.40
135	29.99	291.07	80.44	5.98	0.78	5.49	0.98
138	10.35	294.64	81.59	3.66	0.07	5.59	0.06
Talbot	7.61	282.95	77.84	5.47	0.70	6.84	0.01
117	30.38	282.96	77.33	6.54	0.31	7.18	0.24
290	2.15	282.50	76.36	4.16	0.30	5.98	0.00
290	10.54	282.50	76.36	4.54	0.37	5.72	0.34
292	2.27	279.58	75.85	4.20	0.05	4.51	0.16
292	10.49	279.58	75.85	5.75	0.94	7.28	0.34
site 2.3	1.91	276.98	76.13	4.15	0.31	5.81	0.02
site 2.3	10.13	276.98	76.13	5.19	0.68	5.22	0.48
Site 1.4	1.79	275.06	76.50	4.73	0.37	5.56	0.07
297	1.90	278.70	76.37	5.56	0.08	5.63	0.10
297	10.33	278.70	76.37	5.26	0.03	6.02	0.24
site 2.7	2.35	281.36	75.48	4.00	0.18	5.46	0.24
305A	10.50	266.48	74.22	5.02	0.03	6.55	0.33
108	9.97	285.40	76.26	5.80	0.95	4.29	0.28
126	10.17	286.60	77.35	3.93	0.52	4.68	0.32
126	20.50	286.60	77.35	5.28	0.30	3.91	0.26
132	3.74	287.68	79.00	4.78	0.12	5.21	0.21
132	10.11	287.68	79.00	5.15	0.16	6.19	0.22

132	20.11	287.68	79.00	5.42	1.41	5.37	0.14
133	3.87	289.71	79.58	5.57	0.35	7.31	0.06
133	9.88	289.71	79.58	4.52	0.20	9.61	0.03
136	1.96	292.31	80.36	6.06	0.11	6.88	0.18
136	9.83	292.31	80.36	10.49	0.24	8.21	0.10
135	1.82	291.07	80.44	3.67	0.12	5.48	0.03
135	10.23	291.07	80.44	4.57	0.03	6.03	0.36
137	7.04	293.99	81.07	6.25	3.50	4.52	0.33
138	2.02	294.64	81.59	3.59	0.08	5.85	0.19
117	1.79	282.96	77.33	4.29	0.38	5.31	0.16
117	10.51	282.96	77.33	4.39	0.27	5.36	0.16
Site 1.4	10.77	275.06	76.50	6.45	0.52	6.90	0.48
295	1.92	275.59	76.38	5.45	0.05	3.96	0.18
295	9.98	275.59	76.38	3.55	0.46	4.57	0.48
302	7.17	273.84	74.23	5.18	0.54	6.55	0.33
303	7.27	270.38	74.37	2.74	0.13	3.83	0.40
305A	3.07	266.48	74.22	3.59	0.37	0.81	0.32
305B	3.00	266.44	74.36	4.09	0.18	3.71	0.24
Wel01	2.12	267.61	74.95	4.32	0.22	6.31	1.15
Wel01	9.99	267.61	74.95	5.44	0.40	5.68	0.37
Wel02 327	2.25	266.89	75.01	3.73	0.40	5.58	0.02
Wel02 327	10.04	266.89	75.01	4.38	0.37	5.10	0.17
305 D	2.92	266.28	74.60	4.78	0.30	5.76	0.17
305 D	10.03	266.28	74.60	2.50	0.01	4.48	0.33
190	4.34	298.80	66.59	5.53	0.32	6.71	0.03
190	10.10	298.80	66.59	6.37	0.08	6.21	0.06
190	19.81	298.80	66.59	9.19	0.99	5.57	0.06
190	29.99	298.80	66.59	10.38	0.14	6.12	0.11

193	20.17	300.66	66.77	5.55	0.62	4.54	0.28
196	19.93	303.94	66.99	9.31	0.30	4.60	0.21
198	4.24	305.79	67.08	6.87	0.37	4.57	0.03
198	9.95	305.79	67.08	6.11			
198	19.93	305.79	67.08	8.27	0.35	5.25	0.31
198	30.01	305.79	67.08	7.61	0.57	3.52	0.07
198	68.36	305.79	67.08	7.29	0.40	5.69	0.06
323	20.26	279.53	74.16	27.90	3.15	7.34	0.18
134	9.91	291.55	80.39	5.19	0.00	5.99	0.06
137	30.11	293.99	81.07	6.34	0.01	7.70	0.30
Rob1	20.08	297.64	81.76	4.21	0.30	5.42	0.11
Rob1	29.84	297.64	81.76	4.82	0.10	6.45	0.00
6.4	20.42	296.73	81.62	5.21	0.26	5.97	0.33
6.4	30.23	296.73	81.62	8.88	4.06	5.83	1.66
251b	20.41	298.66	80.97	5.63	0.59	6.34	0.35
Talbot	50.64	282.95	77.84	4.83	0.29	7.09	0.06
293	10.12	279.33	75.73	7.86	0.86	6.57	0.04
296	30.22	280.25	75.52	5.05	0.10	7.25	0.30
302	20.53	273.84	74.23	4.48	0.09	6.23	0.17
302	30.26	273.84	74.23	5.19	1.39	5.25	0.00
305c	20.66	266.36	74.48	6.13	0.29	6.30	0.37
305c	30.73	266.36	74.48	7.46	0.69	6.19	0.31
191	4.18	299.43	66.64	3.46	0.13	6.41	0.27
193	4.23	300.66	66.77	6.03	0.52	5.41	0.12
193	9.97	300.66	66.77	7.37			
196	5.10	303.94	66.99	5.03	0.57	3.43	0.36
196	10.15	303.94	66.99	5.75	0.39	4.43	0.16
198	50.22	305.79	67.08	7.19	0.30	6.00	0.08

BB15	4.45	304.10	68.45	5.24	0.04	4.59	0.62
BB15	10.07	304.10	68.45	4.74	0.15	3.90	0.18
BB15	20.10	304.10	68.45	4.21	0.23	4.17	0.38
BB15	30.10	304.10	68.45	5.41	0.15	3.00	0.26
BB16	3.69	308.13	69.15	4.97	0.04	3.81	0.63
BB16	9.82	308.13	69.15	4.40	0.24	4.47	0.06
BB16	20.21	308.13	69.15	4.83	0.10	4.30	0.22
BB16	29.77	308.13	69.15	4.96	0.31	5.04	0.06
BB18	4.10	307.26	70.09	4.92	0.10	4.77	0.22
228	4.04	305.00	70.90	3.56	0.10	4.69	0.15
228	9.73	305.00	70.90	5.86	0.00	4.17	0.39
228	20.07	305.00	70.90	5.80	0.00	4.55	0.15
229	4.44	306.99	71.00	5.01	0.49	3.73	0.39
227	5.57	303.01	70.80	5.37	0.22	2.95	0.05
227	9.91	303.01	70.80	5.53	0.34	4.80	0.24
226	5.09	300.99	70.70	4.39	0.06	4.18	0.08
226	9.93	300.99	70.70	6.03	0.26	5.00	0.34
224	4.24	297.02	70.44	4.56	0.02	6.55	0.11
223	4.43	295.18	70.27	3.85	0.29	5.19	0.20
223b	4.01	294.20	70.16	5.34	0.23	3.41	0.44
223b	9.91	294.20	70.16	6.54	0.07	5.37	0.27
222	4.14	293.39	70.08	5.40	0.05	3.79	0.36
BB2	4.14	293.00	72.75	4.94	1.41	4.83	0.60
BB2	10.19	293.00	72.75	5.46	0.02	4.62	0.23
201	5.35	298.75	72.50	4.62	0.14	5.72	0.28
204	5.32	302.00	73.27	4.05	0.23	3.92	0.26
210	4.29	298.44	75.42	3.77	0.30	4.84	0.27
210	9.63	298.44	75.42	4.26	1.15	4.87	0.17

BB24	5.61	297.48	75.80	4.98	0.29	3.54	0.45
BB24	9.95	297.48	75.80	4.20	1.07	4.93	0.30
BB24	20.06	297.48	75.80	3.73	0.30	5.06	0.05
115	20.30	288.80	76.33	5.26	0.29	5.34	0.21
111	4.12	286.79	76.31	5.40	0.12	4.76	0.17
108	4.02	285.40	76.26	6.14	0.74	4.94	0.34
105	4.27	284.23	76.32	5.70	0.25	4.80	0.35
105	9.81	284.23	76.32	5.99	1.12	4.95	0.20
101	6.42	282.59	76.38	5.04	0.23	4.45	0.06
322	3.99	279.49	74.49	4.20	0.15	4.26	0.05
322	9.88	279.49	74.49	4.58	0.15	4.76	0.11
323	4.09	279.53	74.16	5.69	0.20	-0.71	0.31
323	10.04	279.53	74.16	5.87	0.05	4.52	0.03
325	4.40	279.49	73.82	3.94	0.07	4.59	0.07
325	9.97	279.49	73.82	4.32	0.02	4.89	0.47
325	20.11	279.49	73.82	5.51	0.50	5.51	0.03
122/site2.8	10.51	284.97	77.34	4.45	0.29	4.55	0.48
122/site2.8	20.19	284.97	77.34	4.90	0.34	6.92	0.15
129	3.89	285.86	78.33	5.40	0.31	4.43	0.30
129	10.45	285.86	78.33	4.89	1.11	4.53	0.22
129	20.14	285.86	78.33	4.24	0.39	5.35	0.49
129	30.36	285.86	78.33	4.67	0.21	4.70	0.79
134	1.81	291.55	80.39	4.70	0.55	5.74	0.98
137	2.22	293.99	81.07	4.04	0.01	5.32	0.12
137	10.15	293.99	81.07	5.91		2.43	
137	20.43	293.99	81.07	4.32	0.26	6.13	0.36
ken 1	1.75	295.81	81.37	4.77	0.12	5.46	0.26
ken 1	10.51	295.81	81.37	4.93	0.44	5.41	0.47

ken 1	20.02	295.81	81.37	3.18	0.13	4.81	0.42
Rob1	2.12	297.64	81.76	6.02	0.58	3.93	0.37
Rob1	10.15	297.64	81.76	4.42	0.62	5.44	0.28
6.4	2.04	296.73	81.62	4.40	0.17	7.88	0.42
6.4	10.38	296.73	81.62	5.32	0.81	3.89	0.23
251b	1.98	298.66	80.97	4.97	0.28	6.46	0.34
251b	10.40	298.66	80.97	4.09	0.03	5.71	0.31
Talbot	1.83	282.95	77.84	3.79	0.05	8.32	0.01
Talbot	10.62	282.95	77.84	7.12	0.17	5.53	0.29
Talbot	20.64	282.95	77.84	3.32	0.14	4.60	0.10
Talbot	29.92	282.95	77.84	5.30	0.12	5.75	0.28
291	2.07	279.63	75.99	4.49	0.08	3.22	0.05
291	9.49	279.63	75.99	5.33	0.17	6.28	0.36
293	1.91	279.33	75.73	3.29	0.21	2.89	0.02
site 2.4	1.89	273.67	76.13	4.46	0.47	5.74	0.07
site 2.4	10.30	273.67	76.13	3.41	0.42	4.89	0.56
site 2.4	20.00	273.67	76.13	5.29	1.06	5.96	0.58
296	2.16	280.25	75.52	4.46	0.08	7.19	0.19
296	10.08	280.25	75.52	5.46	0.50	5.84	0.07
296	19.79	280.25	75.52	4.85	0.64	4.82	0.31
302	2.27	273.84	74.23	2.15	0.63	6.48	0.27
303	3.75	270.38	74.37	4.07	0.24	2.32	0.32
303	10.44	270.38	74.37	4.07	0.00	5.95	0.17
303	19.98	270.38	74.37	11.61	1.16	7.11	0.26
303	30.50	270.38	74.37	4.41	0.71	7.39	0.23
305c	3.22	266.36	74.48	4.85	0.07	7.26	0.07
305c	10.61	266.36	74.48	4.52	0.40	5.72	0.21